Applied Mathematics & Information Sciences **4**(2) (2010), 141–181
– An International Journal

Discrete Systems and Signals on Phase Space

Kurt Bernardo Wolf

Instituto de Ciencias Físicas, Universidad Nacional Autónoma de México
Av. Universidad s/n, Cuernavaca, Morelos 62251, México
Email Address: bwolf@fis.unam.mx

Received January 10, 2010

The analysis of discrete signals —in particular *finite* N-point signals— is done in terms of the eigenstates of discrete Hamiltonian systems, which are built in the context of Lie algebras and groups. These systems are in correspondence, through a 'discrete-quantization' process, with the quadratic potentials in classical mechanics: the harmonic oscillator, the repulsive oscillator, and the free particle. Discrete quantization is achieved through selecting the position operator to be a compact generator within the algebra, so that its eigenvalues are discrete. The discrete harmonic oscillator model is contained in the 'rotation' Lie algebra $\mathsf{so}(3)$, and applies to *finite* discrete systems, where the positions are $\{-j, -j+1, \ldots, j\}$ in a representation of dimension $N = 2j + 1$. The discrete radial and the repulsive oscillator are contained in the complementary and principal representation series of the Lorentz algebra $\mathsf{so}(2,1)$, while the discrete free particle leads to the Fourier series in the Euclidean algebra $\mathsf{iso}(2)$. For the finite case of $\mathsf{so}(3)$ we give a digest of results in the treatment of aberrations as unitary $\mathsf{U}(N)$ transformations of the signals on phase space. Finally, we show two-dimensional signals (pixellated images) on square and round screens, and their unitary transformations.

Keywords: Hamiltonian systems, Quantum mechanics, discrete signals.

1 Introduction

There has been growing interest in discrete and finite Hamiltonian systems to describe models of N-level atoms, mechanical and crystal lattices, granular versions of quantum mechanics, as well as discrete polynomials and special functions in pure mathematics. Our motivation has been to describe the parallel processing of N-point signals by unitary transformations that mimic lossless geometric optical setups, such as is sketched in Figure 1.1. Also, N^2-point two-dimensional images on screens that are pixellated following Cartesian or polar coordinates.

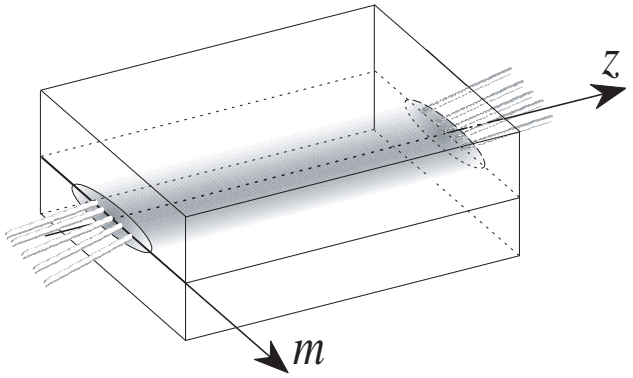

Figure 1.1: Sketch of an optical setup contained in a transparent microchip, where a five-point complex light signal is transformed without loss to a corresponding array of five sensors. Such a discrete Hamiltonian system is expected to register up to five momenta (ray inclinations) and carry five energy states.

Since the mid-1960s, the Fast Fourier transform (FFT) algorithm, which has $\mathcal{O}(N \log N)$ complexity, has allowed the real-time frequency analysis of streaming discrete data, so it has been natural to search the extension of the discrete Fourier transform (DFT) to linear canonical transformations (LCT), which for continuous systems are well understood in the context of quantum mechanics [36, 37, 58, Chapt. 9–10] and optics [23, 45]. Already the group of fractional DFT (FrDFT) presents problems when one asks only that it contain the four powers of the DFT matrix and be unitary [45, Chapt. 6], because it is not uniquely defined from those requirements [41, 69]. Nevertheless, since discrete LCTs are important for signal analysis under Fresnel and discrete-chirp transforms, efforts have been made to find efficient $\mathcal{O}(N \log N)$ algorithms to include the FFT in their computation [32, 48].

In Cuernavaca we have worked with Lie algebras and groups in several of its applications, among them in geometric optics on phase space [63] and in discrete models of quantum mechanics [16]. They are related through a quantization process which is *distinct* from the standard Schrödinger quantization of classical mechanics. The discrete quantization process is designed to preserve the geometry and dynamics of the geometric optical model determined by its two Hamilton equations, and to contract to the classical or Schrödinger quantum models under well-defined limits. The classical systems that we discretize are the harmonic oscillator, the repulsive (or *inverted*) oscillator, and the free particle, according to the Lie algebra that we choose. There is a corresponding phase space of the dimension of the algebra, foliated into quadratic surfaces when definite representations are chosen [1, 6], and which limit to the symplectic plane of the classical models, or to the Wigner-function formalism of quantum mechanics.

In this essay we review the process of discrete quantization as a deformation of the Lie algebra of Poisson brackets between position x, momentum p, and quadratic Hamiltoni-

ans $h^{(\sigma)} = \frac{1}{2}(p^2 + \sigma x^2)$, $\sigma \in \{+1, 0, -1\}$, to the three-dimensional Lie algebras $\mathsf{so}(3)$, $\mathsf{so}(2,1)$, or $\mathsf{iso}(2)$, with commutators between hermitian matrices that represent the observables of position $\mathbf{X}$, momentum $\mathbf{P}$, and a (shifted) Hamiltonian $\mathbf{K}$. The matrices will be of finite dimension $N \times N$ in the first algebra, and infinite in the second two. Exponentiated, they generate unitary matrices that form the groups $\mathsf{SO}(3)$, $\mathsf{SO}(2,1)$ or $\mathsf{ISO}(2)$, of 'translations' in phase space and in time. Prominently, $\mathsf{SO}(3)$ is used in quantum angular momentum theory, where these transformations are rotations in the space of a *multiplet* of $N = 2j + 1$ states ($j \in \mathcal{Z}_0^+$, non-negative integer), such as the spherical harmonics of angular momentum j; the components of these multiplets will be here the entries of the signal N-vectors. In $\mathsf{SO}(2,1)$ the multiplets are infinite, while in $\mathsf{ISO}(2)$ they are plainly the Fourier coefficients of periodic functions. Under these Lie algebra deformations, the classical phase space $(x,\, p) \in \mathsf{R}^2$ deforms to quadratic surfaces within a *meta*-phase space $(x,\, p,\, \kappa^{(\sigma)}) \in \mathsf{R}^3$, namely a sphere, a hyperboloid, or a cylinder, respectively. A covariant Wigner function can be defined on these manifolds with all its desirable properties. The results will apply not only for signals represented by column N-vectors, but to density matrices of entangled states, under bilateral group action.

In Section 2 we detail the discrete quantization process for the three systems that classically have quadratic Hamiltonians, under the ægis of the Lie algebras $\mathsf{so}(3)$, $\mathsf{iso}(2)$, and $\mathsf{so}(2,1)$. We then review the ranges that the discrete position can have within each of these algebras in Section 3, their relation with the value of the Casimir invariant, and we verify that the contraction of the algebras returns the standard continuous quantum and classical systems. The overlaps between the position and energy bases provide the wavefunctions of the discrete system, and in Section 4 we find the finite difference 'Schrödinger' equations that rule the three systems. In Section 5 we write out the $\mathsf{so}(3)$ case of finite signals, where Kravchuk functions are the finite counterparts of the Hermite-Gauss eigenfunctions of the harmonic oscillator. The two $\mathsf{so}(2,1)$ cases are given in Section 6: the discrete radial oscillator in the complementary series of representations, and the discrete repulsive oscillator model. In a short Section 7 we relate the Euclidean algebra $\mathsf{iso}(2)$ of a free particle to the ordinary Fourier series analysis. With these tools we examine in Section 8 the *linear* transformations of N-point signals in $\mathsf{SO}(3)$, as a subgroup of the group $\mathsf{U}(N)$ of all their unitary transformations; those outside $\mathsf{SO}(3)$ count all possible *aberrations* of finite signals. Their nonlinear action is analyzed in the spherical phase space of finite systems, by means of the $\mathsf{SO}(3)$ covariant Wigner function that is detailed in the Appendix.

In Section 9 we construct two-dimensional discrete Hamiltonian systems, modeled by finite screens pixellated along Cartesian and along polar coordinates. We define the Kronecker basis of each pixellation, and bases of definite mode and angular momentum; these correspond to Hermite-Gauss and Laguerre-Gauss beams, and their overlap involves the Clebsch-Gordan coefficients. We apply this to rotate unitarily Cartesian-pixellated images, and to map these on polar-pixellated screens, also unitarily. The concluding Section 10

returns to the context of our research on discrete systems and offers some unsolved problems. The subjects covered in this essay were presented at the International Conference on Mathematics and Information Security (Sohag, Egypt, November 13–15, 2009). This is the reason for the proliferation of citations to the author's work in the bibliography —which is surely incomplete—, and for which I apologize.

2 Geometry and Dynamics in Discrete Quantization

Recall that classical Hamiltonian systems are described by observables of position and momentum $x,\ p$, whose basic *Poisson bracket* is

$$\{x,p\}=1, \tag{2.1}$$

which is skew-symmetric, linearly distributive, and obeys the Leibnitz rule, so it can be extended to all differentiable functions of x,p in the form

$$\{f_1,f_2\}(x,p)=\frac{\partial f_1(x,p)}{\partial x}\frac{\partial f_2(x,p)}{\partial p}-\frac{\partial f_1(x,p)}{\partial p}\frac{\partial f_2(x,p)}{\partial x}. \tag{2.2}$$

Since in particular $\{x,1\}=0$, $\{p,1\}=0$, the quantities x, p, 1 form a *basis* for the Heisenberg-Weyl Lie algebra w [57]. The three systems of our immediate interest are ruled by the quadratic *Hamiltonian* functions

$$h^{(\sigma)}:=\tfrac{1}{2}(p^2+\sigma x^2),\quad \sigma=\begin{cases}+1, & \text{harmonic oscillator,}\\ 0, & \text{free particle,}\\ -1, & \text{repulsive oscillator,}\end{cases} \tag{2.3}$$

that determine the *two Hamilton equations*,

$$\text{geometric:}\qquad \{h^{(\sigma)},x\}=-p, \tag{2.4}$$

$$\text{dynamic:}\qquad \{h^{(\sigma)},p\}=\sigma x. \tag{2.5}$$

The first equation (2.4) is *geometric* because it is true for any classical Hamiltonian of the general form $h^{\rm V}=\frac{1}{2}p^2+V(x)$, while the second equation (2.5) is *dynamic* because in the general case the right-hand side will be $\mathrm{d}V(x)/\mathrm{d}x$. The right-hand side of (2.5) is linear in x, p, $\kappa^{(\sigma)}$ (and 1) only for Hamiltonians with quadratic potentials, so only these can be the generators of a Lie algebra. For $\sigma=+1$, this algebra is the semidirect product of w with rotations $\mathsf{so}(2)$; for $\sigma=-1$, it is with Lorentz boosts $\mathsf{so}(1,1)$, and for $\sigma=0$ with translations $\mathsf{iso}(1)$.

We postulate the following correspondence between the classical observables and (non-commuting) operators in some Hilbert space, with the notation

$$\text{position}\quad x\quad\leftrightarrow\quad \mathcal{X}\equiv\mathcal{L}_0, \tag{2.6}$$

$$\text{momentum} \quad p \quad \leftrightarrow \quad \mathcal{P} \equiv \mathcal{L}_1, \tag{2.7}$$

$$\text{(pseudo) energy } \kappa^{(\sigma)} \quad \leftrightarrow \quad \mathcal{K}^{(\sigma)} \equiv \mathcal{L}_2^{(\sigma)}, \tag{2.8}$$

and $1 \leftrightarrow \mathit{1}$. We shall call $\mathcal{K}$ the *pseudo*-energy —or *mode*— operator because the usual Schrödinger energy will be the eigenvalue of $\mathcal{K} + \gamma \mathit{1}$ (with γ to be determined). And now we replace Poisson brackets of classical coordinates u, v, w, with commutators of operators $\mathcal{U}$, $\mathcal{V}$, $\mathcal{W}$, through $\{u, v\} = w \leftrightarrow [\mathcal{U}, \mathcal{V}] = \mathrm{i}\mathcal{W}$, so that the two Hamilton equations (2.4) and (2.5) translate to

$$[\mathcal{L}_2^{(\sigma)}, \mathcal{L}_0] = -\mathrm{i}\mathcal{L}_1, \quad i.e., \quad [\mathcal{K}^{(\sigma)}, \mathcal{X}] = -\mathrm{i}\mathcal{P}, \tag{2.9}$$

$$[\mathcal{L}_2^{(\sigma)}, \mathcal{L}_1] = \mathrm{i}\sigma\, \mathcal{L}_0, \quad i.e., \quad [\mathcal{K}^{(\sigma)}, \mathcal{P}] = \mathrm{i}\sigma\, \mathcal{X}. \tag{2.10}$$

The second crucial postulate will be now set in place: the deformation of the classical algebras is performed by replacing the basic Poisson bracket (2.1) with the *non-standard* commutator

$$[\mathcal{L}_0, \mathcal{L}_1] = -\mathrm{i}\mathcal{L}_2, \quad i.e., \quad [\mathcal{X}, \mathcal{P}] = -\mathrm{i}\mathcal{K}^{\sigma}. \tag{2.11}$$

The three operators (2.6)–(2.8), with their commutators (2.9)–(2.11), form bases for the following Lie algebras:

$$\mathsf{so}(3) \qquad \text{for } \sigma = +1, \text{ discrete harmonic oscillator,} \tag{2.12}$$

$$\mathsf{so}(2,1) \qquad \text{for } \sigma = -1, \text{ discrete repulsive oscillator,} \tag{2.13}$$

$$\mathsf{iso}(2) \qquad \text{for } \sigma = 0, \quad \text{discrete free particle,} \tag{2.14}$$

in direct sum with the central generator $\mathit{1}$.

The third postulate is to choose the position operator $\mathcal{L}_0 \equiv \mathcal{X}$ to be a *compact* generator in each algebra (and in its corresponding Hilbert space). The Lie-algebraic structure then ensures that its spectrum will be discrete, *i.e.*, that the (observable) positions in the system form a collection of equally-spaced points, $m \in \mathcal{Z}$, finite in $\mathsf{so}(3)$ and infinite in the other two cases [29].

3 Representations, Contractions and Energy

The representations of the Lie algebras (of vector basis $\mathcal{X}$, $\mathcal{P}$, $\mathcal{K}^{(\sigma)}$) are their realizations by matrices ($\mathbf{X}$, $\mathbf{P}$, $\mathbf{K}^{(\sigma)}$), and we are interested in the hermitian *irreducible* ones, that is, those which cannot be further reduced by similarity into diagonal blocks. For the three three-dimensional algebras listed above, their characterization is obtained using the invariant Casimir operators,

$$\mathcal{C}^{(\sigma)} := \sigma\mathcal{X}^2 + \mathcal{P}^2 + \mathcal{K}^2 = \sigma\mathcal{L}_0^2 + \mathcal{L}_1^2 + \mathcal{L}_2^2 = \gamma \mathit{1}, \tag{3.1}$$

where the value of γ essentially determines the irreducible representation (for $\mathsf{so}(2,1)$ an extra dichotomic index is necessary). These matrices act on column vectors, the discrete wavefunctions that we may also call *signals*, or *states* of the system. The states live in complex Hilbert spaces of square-summable sequences ℓ^2 over the integers $\mathcal{Z}$, or over $\mathcal{Z}_0^+$, or C^N for finite dimension N, with the usual inner product and norm,

$$(f,g) := \sum_{m\in\Sigma(\mathcal{X})} f_m^* \, g_m = (g,f)^*, \qquad |f| := \sqrt{(f,f)}, \tag{3.2}$$

where $\Sigma(\mathcal{X})$ is the spectrum of $\mathcal{X}$.

The simultaneous eigenbasis of the compact position generator of the algebra, $\mathcal{X} = \mathcal{L}_0$, and of the Casimir operator (3.1), is the Kronecker basis for the system,

$$\mathcal{X}\, f_m^\gamma = m\, f_m^\gamma, \quad m\in\mathcal{Z}, \qquad \mathcal{C}^{(\sigma)}\, f_m^\gamma = \gamma\, f_m^\gamma, \tag{3.3}$$

so $\{f_m\}_{m\in\Sigma(\mathcal{X})}$ are column vectors of 0's with a single 1 at position m. For the three algebras under consideration, the spectra $\{\gamma\} = \Sigma(\mathcal{C}^{(\sigma)})$ and $\{m\} = \Sigma(\mathcal{X})$ are [22,29,42]

$$\begin{array}{ll} \mathsf{so}(3) & \gamma = j(j+1), \quad j\in\mathcal{Z}_0^+, \quad |m|\le j, \\ \sigma{=}1 & \text{representation of dimension } N = 2j+1; \end{array} \tag{3.4}$$

$$\begin{array}{ll} \mathsf{so}(2,1) & \gamma = k(1-k) < \tfrac{1}{4}, \quad k\in\mathcal{Z}^+, \quad m\in\pm\{k,\, k{+}1,\ldots\}, \\ \sigma=-1 & \text{complementary series } D_\pm^k, \end{array} \tag{3.5}$$

$$\begin{array}{l} \gamma = k(1-k) \ge \tfrac{1}{4}, \quad k = \tfrac{1}{2}{+}\mathrm{i}\kappa,\ \kappa\in\mathsf{R}, \quad m\in\mathcal{Z}, \\ \text{principal series } C_0^\kappa; \end{array} \tag{3.6}$$

$$\begin{array}{ll} \mathsf{iso}(2) & \gamma = l^2, \quad l\in\mathsf{R}, \quad m\in\mathcal{Z}, \\ \sigma=0 & \text{infinite-dimensional representation.} \end{array} \tag{3.7}$$

This list is incomplete because when these Lie algebras are exponentiated to the corresponding Lie groups, they have *covers*: $\mathsf{SO}(3) \overset{1:2}{=} \mathsf{SU}(2)$, $\mathsf{SO}(2,1) \overset{1:2}{=} \mathsf{SU}(1,1) = \mathsf{Sp}(2,\mathsf{R}) = \mathsf{SL}(2,\mathsf{R}) \overset{1:\infty}{=} \overline{\mathsf{Sp}}(2,\mathsf{R})$, and $\mathsf{ISO}(2) \overset{1:\infty}{=} \overline{\mathsf{ISO}}(2)$. The first, $\mathsf{SU}(2)$, can have also half-integer $\{m\}$ spectra, while the infinite covers exhibit integer-spaced m's on any real values (additionally, $\mathsf{SO}(2,1)$ has the *supplementary series* in the interval $0<k<1$). We shall thus only consider representations where $m=0$ is a position point of the discrete system.

As we promised above we should show that under contraction, when the discrete position points come closer together until they are dense in the continuum, the discrete systems described by (3.4)–(3.7) become the usual quantum mechanical harmonic and repulsive oscillators, and the free particle. First we prove this for the algebras, and then for the Hamiltonians. Dropping σ as superindex, let

$$\mathcal{X}_\gamma := \gamma^{-1/4}\mathcal{X}, \quad \mathcal{P}_\gamma := \gamma^{-1/4}\mathcal{P}, \quad \mathcal{K}_\gamma := \mathcal{K} + \gamma^{1/2}\mathcal{1}, \tag{3.8}$$

where γ is the value of the Casimir operator (3.1). When $\gamma \to \infty$, the two Hamilton equations (2.9)–(2.10) remain invariant (as they should), while the nonstandard commutator (2.11) becomes

$$[\mathcal{X}_\gamma, \mathcal{P}_\gamma] = \frac{1}{\sqrt{\gamma}}[\mathcal{X}, \mathcal{P}] = -\frac{\mathrm{i}}{\sqrt{\gamma}}(\mathcal{K}_\gamma - \sqrt{\gamma}\,\mathit{1}) \;\xrightarrow[\gamma\to\infty]{}\; \mathrm{i}\mathit{1}, \tag{3.9}$$

weakly, in the subspace of ℓ^2 states $\mathbf{f} = \{f_m\}$ such that $(f,\, \mathcal{K}^2 f) < \infty$, *i.e.*, signals of bounded energy as defined below. Next, we write (3.1) as

$$\begin{aligned} \gamma\mathit{1} &= \sqrt{\gamma}\mathcal{P}_\gamma^2 + \sigma\sqrt{\gamma}\mathcal{X}_\gamma^2 + (\mathcal{K}_\gamma - \sqrt{\gamma}\mathit{1})^2 \\ &= \sqrt{\gamma}(\mathcal{P}_\gamma^2 + \sigma\mathcal{X}_\gamma^2 - 2\mathcal{K}_\gamma) + \mathcal{K}_\gamma^2 + \gamma\mathit{1}, \qquad (3.10) \\ \Longrightarrow \qquad \mathcal{K}_\gamma &= \tfrac{1}{2}(\mathcal{P}_\gamma^2 + \sigma\mathcal{X}_\gamma^2) + \frac{1}{2\sqrt{\gamma}}\mathcal{K}_\gamma^2, \qquad (3.11) \end{aligned}$$

which becomes the Schrödinger version of (2.3), with the same condition of validity. This also indicates that the eigenvalues η of $\mathcal{K}_\gamma$ are related to the eigenvalues λ of $\mathcal{K}$ through $\mathcal{K}_\gamma = \mathcal{K} + \mathit{1}\sqrt{\gamma}$. Thus, the relation between energy and pseudo-energy has the generic form

$$\eta \approx \lambda + \sqrt{\gamma} + \text{constant}. \tag{3.12}$$

4 'Schrödinger' Difference Equations

Continuous quantum mechanical systems evolve obeying Schrödinger second-order differential equations, which are determined by their Hamiltonian, where the momentum operator is realized as $-\mathrm{i}\hbar\mathrm{d}/\mathrm{d}x$, and position by x, which thus relate three infinitesimally near points of space. The discrete systems introduced here are a pre-contracted version of those, and so obey a finite difference equation that relates the values, in each pseudo-energy eigenstate, of three neighboring points spaced by unity,

$$\mathcal{K}\, h_\lambda^\gamma = \lambda\, h_\lambda^\gamma, \quad \lambda \in \Sigma(\mathcal{K}), \qquad \mathcal{C}\, h_\lambda^\gamma = \gamma\, h_\lambda^\gamma. \tag{4.1}$$

The *wavefunctions* of the discrete system will then be the *overlaps* between the Kronecker position eigenbasis (3.3) and the energy basis (4.1), namely

$$\Psi_\lambda^\gamma(m) := (f_m^\gamma,\, h_\lambda^\gamma). \tag{4.2}$$

To find this 'Schrödinger' difference equation, one uses the raising and lowering operators

$$\mathcal{L}_\uparrow := \mathcal{K} + \mathrm{i}\mathcal{P}, \qquad \mathcal{L}_\downarrow := \mathcal{K} - \mathrm{i}\mathcal{P}. \tag{4.3}$$

From (2.9)–(2.11), their commutators are $[\mathcal{L}_0, \mathcal{L}_\updownarrow] = \pm\mathcal{L}_\updownarrow$ and $[\mathcal{L}_\uparrow, \mathcal{L}_\downarrow] = 2\sigma\mathcal{L}_0$. Their role is to shift the position of the Kronecker states (3.3) up and down by one unit,

$$\mathcal{L}_{\uparrow\downarrow}\, f_m^\gamma = c_{\uparrow\downarrow\, m}^\gamma\, f_{m\pm1}^\gamma. \tag{4.4}$$

The normalization constants $c^\gamma_{\uparrow\downarrow\, m}$ can be found through a well-known line of reasoning [29] that involves writing the Casimir invariant (3.1) as $\mathcal{C} = \mathcal{L}_{\uparrow\downarrow}\mathcal{L}_{\downarrow\uparrow} + \mathcal{L}_0(\mathcal{L}_0 \pm 1)$ and applying it to f^γ_m. The result is

$$c^\gamma_{\uparrow\, m} = \varphi_{\uparrow\, m}\sqrt{\gamma - \sigma m(m{+}1)}, \quad c^\gamma_{\downarrow\, m} = \varphi_{\downarrow\, m}\sqrt{\gamma - \sigma m(m{-}1)}, \tag{4.5}$$

with phases that can be of the general form $\varphi_{\uparrow\, m} = e^{\mathrm{i}\alpha m}$ and $\varphi_{\downarrow\, m} = e^{-\mathrm{i}\alpha(m-1)}$, with α modulo 2π at our choosing, but subject to convention [22, 29] to $\alpha = 0$. Then, (4.1) and (4.4) with $2\mathcal{K} = \mathcal{L}_\uparrow + \mathcal{L}_\downarrow$, lead to the following three-term difference equation in discrete position

$$\sqrt{\gamma - \sigma m(m{+}1)}\,\Psi^\gamma_\lambda(m{+}1) + 2\lambda\Psi^\gamma_\lambda(m) + \sqrt{\gamma - \sigma m(m{-}1)}\,\Psi^\gamma_\lambda(m{-}1) = 0. \tag{4.6}$$

This difference equation contracts under (3.8)–(3.12) to the Schrödinger equations: denoting the eigenvalues of $\mathcal{X}$ by m, those of $\mathcal{X}_\gamma$ by $x := \gamma^{-1/4}m$, and re-defining $\psi(x) = \psi(\gamma^{-1/4}m) := \Psi^\gamma_\lambda(m)$, for γ large and $\delta := \gamma^{-1/4}$, we expand (4.6) to order δ^2 and approximate using x-derivatives,

$$\Psi^\gamma_\lambda(m \pm 1) = \psi(x \pm \delta) \;\approx\; \psi(x) \pm \delta\,\psi'(x) + \tfrac{1}{2}\delta^2\,\psi''(x), \tag{4.7}$$

$$\sqrt{\gamma - \sigma m(m{\pm}1)} \;\approx\; \sqrt{\gamma} - \tfrac{1}{2}\sigma x^2 \mp \delta\,\sigma x - \tfrac{1}{8}\delta^2\,x^4. \tag{4.8}$$

Replacing into (4.6) and truncating to order δ^2, the $\gamma \to \infty$ limit is

$$\tfrac{1}{2}(-\psi''(x) + \sigma x^2\,\psi(x)) = (\lambda + \sqrt{\gamma})\,\psi(x) = \eta\,\psi(x), \tag{4.9}$$

i.e., the time-independent Schrödinger equation of the corresponding quadratic system.

In the following sections we shall show separately the wavefunctions of the three one-dimensional systems of our concern: the finite $\mathsf{so}(3)$ harmonic oscillator, the two $\mathsf{so}(2,1)$ cases of the discrete radial and repulsive oscillators, and the $\mathsf{iso}(2)$ discrete free particle. Then, their respective phase spaces will be given, and finally some comments on the current progress in two-dimensional images will be cited.

5 The $\mathsf{so}(3)$ Finite Oscillator

The Lie algebra $\mathsf{so}(3)$ is the only *compact* three-dimensional one, and the finite harmonic oscillator thus serves for the analysis of N-point finite signals $\{F_m\} = \mathbf{F} \in \mathsf{C}^N$ of complex values. We shall treat $N = 2j + 1$ to be an odd number (j positive integer) with a symmetric range of positions $-j \le m \le j$, so that the center $m = 0$ be in the sensor set. The difference equation (4.6) can be compared with the solutions to the standard Wigner $\mathsf{so}(3)$ recursion relation [22, Eqs. (3.83)],

$$\sqrt{(j{-}m)(j{+}m{+}1)}\,\psi^j_\lambda(m{+}1) + 2\lambda\psi^j_\lambda(m) + \sqrt{(j{+}m)(j{-}m{+}1)}\,\psi^j_\lambda(m{-}1) = 0, \tag{5.1}$$

where the coefficient of $\psi^j_\lambda(m{+}1)$ vanishes for $m = j$ and that of $\psi^j_\lambda(m{-}1)$ for $m = -j$, so that the discrete oscillator wavefunctions are zero for $|m| > j$.

The coefficients that relate the spherical harmonics refered to two colatitude axes separated by an angle β are the Wigner *little-d* functions $d^j_{m,m'}(\beta)$; in our case, the position and energy axes, x- and κ, are orthogonal; we thus recognize the solutions of the difference equation (5.1) to be

$$\Psi^j_n(m) \;:=\; d^j_{\lambda,m}(\tfrac{1}{2}\pi) \qquad\qquad n := \lambda + j \in [0, 2j] \tag{5.2}$$

$$\;=\; \frac{(-1)^n\,(2j)!\,{}_2F_1(-n,\,-2j{-}m;\,-2j;\,2)}{2^j\sqrt{n!\,(2j{-}n)!\,(j{+}m)!\,(j{-}m)!}} \tag{5.3}$$

$$\;=\; \frac{(-1)^n}{2^j}\sqrt{\binom{2j}{n}\binom{2j}{j+m}}\;K_n(j{+}m;\,\tfrac{1}{2},\,2j). \tag{5.4}$$

The discrete position coordinate is $-j \le m \le j$, the state *mode* is n, and energy (3.12) is $\eta := n + \frac{1}{2}$ [16]. The expression (5.4), found by Atakishiyev and Suslov [15], factors the m-dependence of the Wigner-d into a symmetric *Kravchuk polynomial* of degree n [14,15],

$$K_n(j{+}m;\tfrac{1}{2},2j) = {}_2F_1(-n,\,-2j{+}m;-2j;2) = K_{j+m}(n;\tfrac{1}{2},2j), \tag{5.5}$$

and the square root of a binomial. When contracted by $j \to \infty$, the former become Hermite polynomials and the latter a Gaussian factor. As shown in [12], upon writing $m = x\sqrt{j}$,

$$\lim_{j\to\infty}(-1)^m j^{1/4}\Psi^j_n(m) = e^{-x^2/2}H_n(x)\Big/\sqrt{2^n n!\,\sqrt{\pi}}. \tag{5.6}$$

We will refer to $\{\Psi^j_n(m)\}_{n=0}^{2j}$ as the *modes* of the finite harmonic oscillator.

Please note that in the overlap (4.2) and in the ensuing discussion leading to the difference equation (5.1), we can permute the axes $\{\mathcal{L}_i\}$ through $0 \to 2 \to 1 \to 0$, and thus obtain a difference equation relating three neighboring *energy* wavefunctions, $\Psi^j_n(m)$ and $\Psi^j_{n\pm1}(m)$, exchanging only $m \leftrightarrow \lambda = n - j$; *i.e.*, $\Psi^j_n(m) = \Psi^j_{m+j}(n-j)$. The Wigner little-$d$'s have many symmetry and other properties. In particular note carefully that for integer $n \in [0, 2j]$, $\Psi^j_n(m)$ is an *analytic* function of m —being the product of a polynomial and the square root of a binomial— with branchpoint zeros at the integers $|m| > j$. Conversely, for integer $|m| \le j$, it is a similar analytic function of n.

In Figure 5.1 we show the finite harmonic oscillator wavefunctions $\Psi^j_n(m)$ for $N = 65$ points $\{m\}$ and selected numbers n near to the bottom, center and top of this $j = 32$ multiplet. These wavefunctions are real, orthogonal and complete in C^N. Another useful representation of the whole basis is provided by a density plot of the matrix $\mathbf{\Psi}^j = \|\Psi^j_n(m)\|$, shown in Figure 5.2; as we remarked above, this matrix is symmetric across the diagonal. The finite oscillator wavefunctions form a privileged basis from which a density-matrix description of entangled states can be made. Under $\mathsf{SO}(3)$ rotations, the states (5.2) will transform among themselves irreducibly, with the same Wigner '*big-D*'

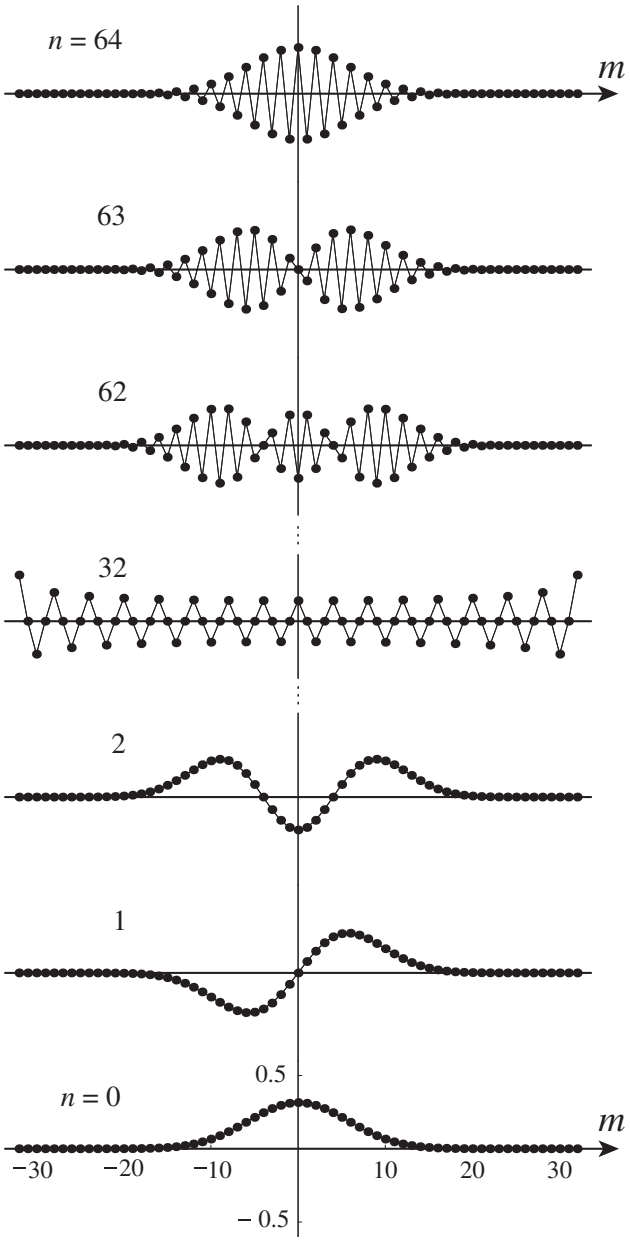

Figure 5.1: Finite oscillator wavefunctions $\Psi^j_n(m)$ for $N = 65$ points. From bottom to top, $n = 0, 1, 2, \ldots, 32, \ldots, 62, 63, 64 = 2j$.

coefficients $D^j_{m,m'}(\alpha, \beta, \gamma)$ as the spherical harmonics [29]. Time evolution is generated by $\exp[-\mathrm{i}\tau(\mathcal{K} + j + \frac{1}{2})]$, which multiplies $\Psi^j_n(m)$ by the phase $\exp[-\mathrm{i}\tau(n + \frac{1}{2})]$.

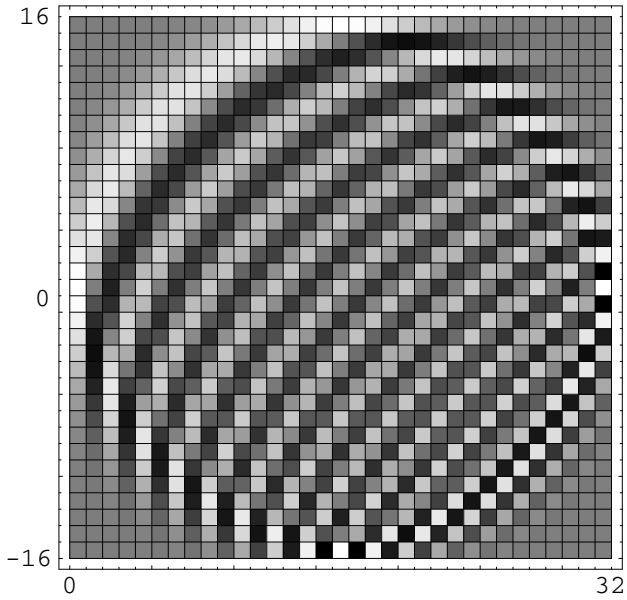

Figure 5.2: The finite oscillator basis represented through the density plot of the matrix $\|\Psi^j_{n(m)}\|$, on the horizontal axis $n \in [0, 2j]$, and vertical axis $m \in [-j, j]$, for $j = 16$, *i.e.*, for $2j + 1 = 33$-point systems.

The ground state of the finite oscillator is

$$\Psi^j_{0(m)} = d^j_{-j,m}(\tfrac{1}{2}\pi) = \frac{1}{2^j}\sqrt{\frac{(2j)!}{(j+m)!\,(j-m)!}}, \tag{5.7}$$

while the top state $\Psi^j_{2j(m)} = (-1)^m \Psi^j_{0(m)}$ is the highest-energy waveform that the finite system can carry. As with the quantum oscillator ground state, all coherent states are obtained through translation —here $\mathsf{SO}(3)$ *rotation*— of phase space [14, 69]. This indicates that a *sphere* will be the proper phase space for finite hamiltonian systems, as we shall elaborate below, after we present the wavefunctions of the $\mathsf{SO}(2,1)$ and $\mathsf{ISO}(2)$ discrete systems. Another point which merits consideration is that the finite oscillator difference equation (5.1), stemming from $\mathcal{K} = \frac{1}{2}(\mathcal{L}_\uparrow + \mathcal{L}_\downarrow)$, does not separate into a sum of kinetic and potential energy terms. However, an 'equivalent potential' can be defined from (5.7), since the ground state has no zeros, as its normalized second-difference $\Delta\Psi^j_{0(m)}/\Psi^j_{0(m)}$. As expected, this yields a parabola-like discrete form [62].

6 The Two $\mathsf{so}(2,1)$ Cases

$\mathsf{so}(2,1)$ is a *non-compact* Lie algebra; the representative of its only compact generator will be the position operator $\mathcal{X}$ whose spectrum is discrete; the pseudo-energy operator

$\mathcal{K}$ can have discrete or continuous spectra according to the eigenvalue $\gamma = k(1-k)$ of the Casimir operator [see (3.7)], in the complementary lower-bound D^k_+ when $\gamma < \frac{1}{4}$ (extended to continuous $k > 0$); or in the principal C^κ_0 series of $\mathsf{so}(2,1)$ representations when $\gamma \geq \frac{1}{4}$, $k = \frac{1}{2} + \mathrm{i}\kappa$ ($\kappa \in \mathsf{R}$). The two cases have been investigated in different contexts. First, for D^k_+ in (3.5), we give the results of Ref. [9] regarding a discrete radial harmonic oscillator (or a one-dimensional oscillator with centrifugal force). And second, for C^κ_0 in (3.6), we return with the discretization philosophy applied to the one-dimensional repulsive oscillator system following Ref. [39].

6.1 Discrete radial oscillator

The framework for a discrete analogue of the radial part of a D-dimensional harmonic oscillator is based on the group of linear canonical (symplectic) transformations of ordinary quantum-mechanical phase space [38, 56], reduced with respect to D-dim rotations,

$$\mathsf{Sp}(2D,\mathsf{R}) \supset \mathsf{SO}(D) \otimes \mathsf{Sp}(2,\mathsf{R}). \tag{6.1}$$

On the right-hand side, the two groups are complementary, *i.e.*, within one representation of $\mathsf{Sp}(2D,\mathsf{R})$, the representation of the *angular* subgroup $\mathsf{SO}(D)$, determines the representation of the *radial* subgroup $\mathsf{Sp}(2,\mathsf{R})$.

In the plane $D = 2$ case, the rotation subgroup is $\mathsf{SO}(2)$ with eigenfunctions $\sim e^{\mathrm{i}a\phi}$, integer a being the angular momentum; but its infinite cover $\overline{\mathsf{SO}}(2)$ is the translation group, where a can be real. Separating the continuous variables of radius $r \in \mathsf{R}^+$ from angle ϕ, the Hamiltonians of the three quadratic systems we are treating generate a realization of the 'radial' Lie algebra $\mathsf{so}(2,1) \equiv \mathsf{sp}(2,\mathsf{R})$, given by *second*-order differential operators,[1]

$$\widehat{J}^{(k)}_0 := \tfrac{1}{4}\Big(-\frac{\mathrm{d}^2}{\mathrm{d}r^2} + \frac{a^2-\frac{1}{4}}{r^2} + r^2\Big), \qquad \widehat{J}^{(k)}_1 := \tfrac{1}{4}\Big(-\frac{\mathrm{d}^2}{\mathrm{d}r^2} + \frac{a^2-\frac{1}{4}}{r^2} - r^2\Big), \tag{6.2}$$

$$\widehat{J}^{(k)}_2 := -\mathrm{i}\tfrac{1}{2}\Big(r\frac{\mathrm{d}}{\mathrm{d}r} + \tfrac{1}{2}\Big), \qquad i.e.\ \widehat{J}^{(k)}_- := \widehat{J}^{(k)}_0 - \widehat{J}^{(k)}_1 = \tfrac{1}{2}r^2. \tag{6.3}$$

The relation between $a \geq 0$ and the *Bargmann* index k is evinced by the Casimir operator (3.1) of this realization,

$$\begin{aligned} \widehat{\mathcal{C}} = \gamma 1, \qquad & \gamma = \tfrac{1}{4}(1-a^2) = k(1-k), \\ \text{for} \qquad & a = 2k-1, \quad k := \tfrac{1}{2}(a+1) \geq \tfrac{1}{2}, \end{aligned} \tag{6.4}$$

exactly as in (3.5). These operators are essentially self-adjoint in a Hilbert space $\mathcal{L}^2(\mathsf{R}^+)$ with measure $\mathrm{d}r$. They exponentiate into the group of unitary 'radial' canonical integral transformations (including fractional Hankel transforms), whose complex extension was analyzed in [56].

[1] Classical Lie theory deals only with first-order differential operators; the only semisimple algebras one can realize with second-order differential operators are the real symplectic algebras of dimension D.

The compact generator $2\widehat{J}_0^{(k)}$ in (6.2) is a harmonic oscillator plus a centrifugal potential C/r^2, with coefficient $C := a^2 - \frac{1}{4} \geq -\frac{1}{4}$ for $k \geq \frac{1}{2}$. In $\mathsf{so}(2,1)$, the *exceptional interval* is $0 \leq k < 1$, which includes *weak* barriers $0 < C < \frac{3}{4}$, *weak* wells $-\frac{1}{4} < C < 0$, and $C = 0$; in this interval, the operators do *not* have a unique self-adjoint extension, but again we simplify matters by taking the Friedrichs extension, where the spectrum of this oscillator + centrifugal Hamiltonian $2\widehat{J}_0^{(k)}$ is equally spaced and given by $\eta := n + k$, $n \in \mathcal{Z}_0^+$ [66]. For all representations the 'square-radial' position operator is $\widehat{J}_-^{(k)} = \frac{1}{2}r^2$ in (6.3), which is diagonal, non-compact, and with a simple spectrum $\frac{1}{2}r^2 \geq 0$ for $r \geq 0$. The eigenfunctions of $2\widehat{J}_0^{(k)}$ in this realization are the well-known Laguerre-Gauss functions that will appear below [in (6.12)].

We *do* want equally-spaced energies, but to have a *discrete* system, we must choose some other compact $\mathsf{so}(2,1)$ generator —distinct from $\widehat{J}_0^{(k)}$ but with a limit to $\widehat{J}_-^{(k)}$— to be our square-radial position operator. This we can achieve with a diagonal scaling transform [9], defining for every k and $\zeta > 0$, the 'discrete square-radial' operators

$$\begin{aligned} \widehat{J}_{(\zeta)} &:= e^{-\zeta} \exp(\mathrm{i}\zeta \widehat{J}_2)\, \widehat{J}_0\, \exp(-\mathrm{i}\zeta \widehat{J}_2) \\ &= e^{-2\zeta}\tfrac{1}{4}\Big(-\frac{\mathrm{d}^2}{\mathrm{d}r^2} + \frac{a^2-\frac{1}{4}}{r^2}\Big) + \tfrac{1}{4}r^2, \end{aligned} \tag{6.5}$$

whose $\zeta \to \infty$ limit is clearly $\widehat{J}_{(\infty)} = \frac{1}{2}\widehat{J}_- = \frac{1}{4}r^2$.

The overlaps between the eigenfunctions of energy, ψ_n^k of $2\widehat{J}_0$ with eigenvalue $\lambda = k+n$ ($n \in \mathcal{Z}_0^+$), and the Kronecker eigenbasis of position, $\psi_{\zeta,m}^k$ of $2\widehat{J}_{(\zeta)}$, with eigenvalues $\mu = k + m$ ($m \in \mathcal{Z}_0^+$), on the square-radial positions $r_m^2 \approx 2e^{-\zeta}m \geq 0$, are

$$\Psi_n^{k,\zeta}(m) := (\psi_{\zeta,m}^k,\, \psi_n^k) \tag{6.6}$$

$$= (\exp[\mathrm{i}\zeta\widehat{J}_2]\psi_m^k,\, \psi_n^k) = (\psi_m^k,\, \exp[-\mathrm{i}\zeta\widehat{J}_2]\psi_n^k) \tag{6.7}$$

To find this overlap, we use the raising and lowering operators as in (4.3) with the $\widehat{J}_i$'s instead of $\mathcal{L}_i$'s, and follow (4.4)–(4.6) to find the difference equation for $\Psi_n^{k,\zeta}(m)$ that relates three neighboring points in space, m and $m \pm 1$. Recalling that $\mu := k + m$ and $\lambda := k + n$, this is

$$\begin{aligned} \sqrt{(m+1)(2k+m)}\,\Psi_n^k(m{+}1) + 2(k{+}n)\,\Psi_n^k(m) \\ + \sqrt{m(2k+m-1)}\,\Psi_n^k(m{-}1) = 0 \end{aligned} \tag{6.8}$$

We see that the second coefficient $c_{\downarrow,\,\mu=k}^k = 0$ provides the zero boundary condition for $m < 0$ in the D_+^k representation series (the upper-bound series D_-^k contains all $m \leq 0$). The boundary condition at zero determine uniquely the solution to (6.8), which is also known in the guise of the Bargmann $\mathsf{SO}(2,1)$ little-d function $d_{k+m,k+n}^k(\zeta)$ [18]; this is none other but the unitary irreducible representation matrix of the boost between the two bases (6.6). Several expressions for it exist, among them one that displays them in

terms Meixner polynomials, found by Atakishiyev and Suslov [15]. Using the parameter $\xi := \tanh^2 \frac{1}{2}\zeta \in (0,1)$, this displays the discrete radial oscillator wavefunctions as

$$\Psi_n^{k,\zeta}(m) \;:=\; d^k_{k+m,k+n}(\zeta) = \Psi_m^{k,\zeta}(n) \qquad m,n \in \mathcal{Z}_0^+ \tag{6.9}$$

$$\;=\; \sqrt{\frac{\xi^{n+m}(1-\xi)^{2k}\,(2k)_n\,(2k)_m}{n!\,m!}}\; M_n(m;\,2k,\,\xi), \tag{6.10}$$

where $(a)_n = \Gamma(a+n)/\Gamma(a)$ is the Pochhammer symbol, and the Meixner polynomial of degree n in m is

$$M_n(m;\,2k,\,\xi) = {}_2F_1\Big(\begin{matrix}-n,\,-m\\ 2k\end{matrix};\,1-\frac{1}{\xi}\Big) = M_m(n;\,2k,\,\xi). \tag{6.11}$$

We should be aware from (6.5) and the text below, that the discrete points $m \geq 0$ now correspond to discrete radii $r_m = 2e^{-\zeta/2}\sqrt{m}$. These functions are orthogonal and complete in the Hilbert space $\ell^2(\mathcal{Z})$ of square-summable sequences, and form also a symmetric, but now half-infinite matrix. And again note carefully that for integer $n \in \mathcal{Z}_0^+$, $\Psi_n^k(m)$ is an analytic function of m with branchpoint zeros at the negative integers; and conversely for $m \in \mathcal{Z}_0^+$ as a function of n.

In Figure 6.1 we show discrete radial oscillator wavefunctions $\Psi_n^{k,\zeta}(m)$ in (6.10) for various values of a, n, ζ, while in Figure 6.2 we show the density plot of a part of the whole, infinite basis. We understand that as ζ grows, the radii r_m come closer together and the approximation to the Laguerre-Gauss wavefunctions improves. Indeed, the $\zeta \to \infty$ limit relation is [9]

$$\lim_{\zeta\to\infty} \frac{1}{\sqrt{2}}\, e^{\zeta/2}\Psi_n^{k,\zeta}(\tfrac{1}{4}e^{\zeta}r^2) = \sqrt{\frac{2\,n!}{(a+n)!}}\; e^{-r^2/2} r^{a+1/2}\, L_n^a(r^2), \tag{6.12}$$

with $a = 2k-1$. Comparing this limit with the $\gamma \to \infty$ limit in (4.9) and (5.6), we see that here ζ is a contraction parameter independent of the representation.

6.2 Discrete repulsive oscillator wavefunctions

We return to the main line of reasoning to discretize quadratic Hamiltonian systems, namely (2.6)–(2.8) for the case (2.13) of the repulsive oscillator. The energy spectrum of this system is the full real line, $\eta \in \mathsf{R}$, but the set of positions will be discrete and infinite, $m \in \mathcal{Z}$, so we must use the representations (3.6) in the principal series C_0^κ where $k = \frac{1}{2}+\mathrm{i}\kappa$ and $\gamma = \kappa^2 + \frac{1}{4}$, labelled by $\kappa \in \mathsf{R}$. There are several reasons for investigating the discrete wavefunctions that converge to the quantum repulsive oscillator wavefunctions [58, Sects. 7.5.11–15]: it is a discrete but Dirac-orthonormal basis for $\ell^2(\mathcal{Z})$ in the pseudo-energy label λ; there is a classical distinction between negative- and positive-energy states, which reflect or pass over the potential barrier, but tunneling should occur under quantization; the

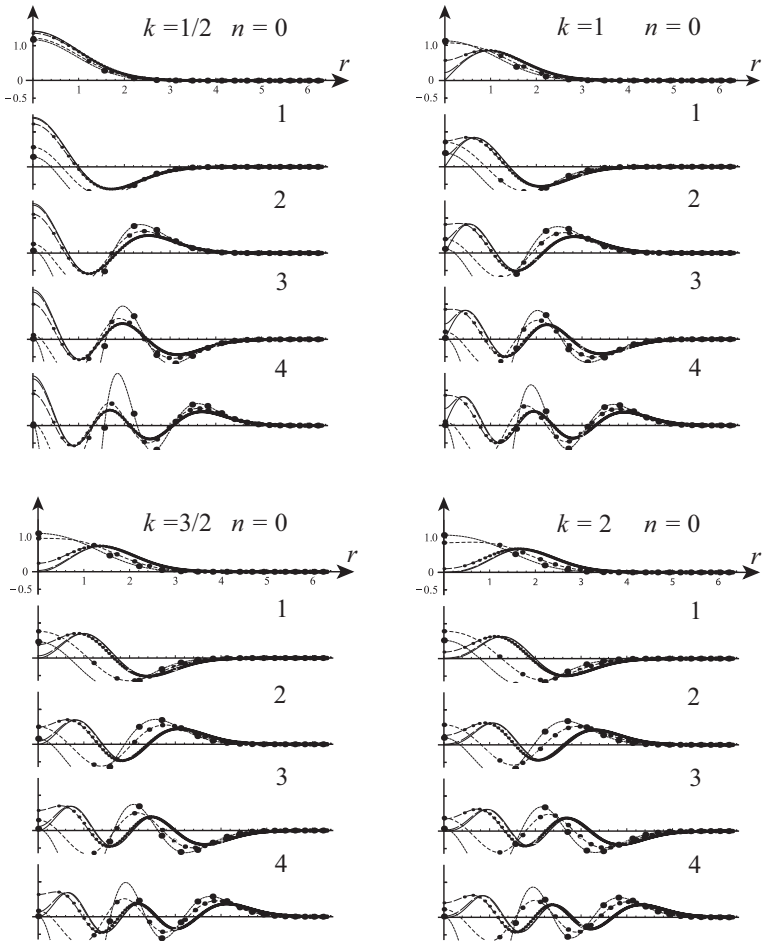

Figure 6.1: Eigenfunctions of the discrete harmonic oscillator with a centrifugal potential, $\Psi_n^{k,\zeta}(m)$ in (6.10), with angular momenta $a = 2k - 1$ shown in *(a)*: For $a = 0$ ($k = \frac{1}{2}$), *(b)*: $a = 1$ ($k = 1$), *(c)*: $a = 2$ ($k = \frac{3}{2}$). Each graph contains successive refinements of the set of orthogonality points $r_m^2 = 4e^{\zeta}m$, for $\zeta = 0.5,\ 1,\ 3,\ 5,\ \infty$, marked by bullets of decreasing size, interpolated (since they are analytic functions of m) by dashings that converge to the continuum Laguerre-Gauss functions. From top to bottom, the radial modes $n = 0, 1, 2, 3, 4$.

quantum wavefunctions behave as chirps $\sim \exp(\mathrm{i}ax^2)$ for large x, yet discrete signals are bound by an upper frequency.

The constants (4.5) in this case are all nonzero; in (4.6) they yield the difference equation

$$\sqrt{(m+\tfrac{1}{2})^2+\kappa^2}\,\psi_\lambda^\kappa(m+1) - 2\lambda\psi_\lambda^\kappa(m) + \sqrt{(m-\tfrac{1}{2})^2+\kappa^2}\,\psi_\lambda^\kappa(m-1) = 0. \qquad (6.13)$$

This equation has two independent solutions, which may be separated into right- and left-

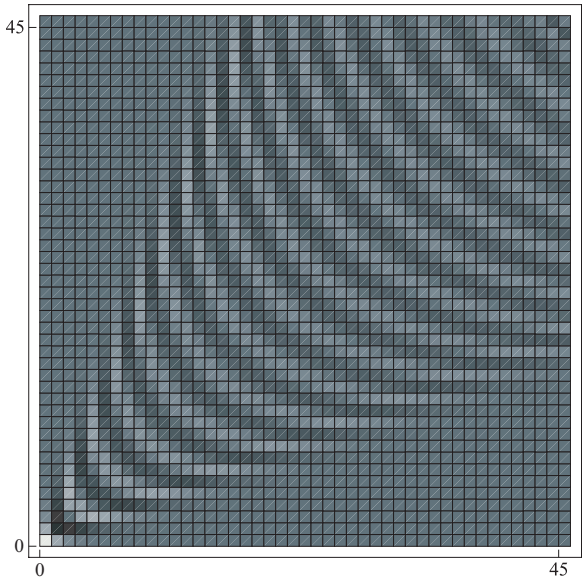

Figure 6.2: The discrete centrifugal oscillator basis represented through a density plot of the matrix $\|\Psi_n^{k,\zeta}(m)\|$ in (6.10), for $\zeta = 1$, $k = \frac{1}{2}$ (angular momentum $a = 0$), and $n, m \in \mathcal{Z}_0^+$ shown up to $n, m \leq 45$. The figure is symmetric under $n \leftrightarrow m$, so the axes are exchangeable. Compare with Fig. 5.2.

moving waves, as determined by their values at two points, $m = 0$ and 1 for example. How to separate them? From previous work we recognize that the $\Psi_\lambda^\kappa(m)$'s are the overlaps between the Kronecker eigenbasis of position $\mathcal{L}_0$ and the Dirac basis of pseudo-energy $\mathcal{L}_2$, which was computed solving integrals in Ref. [20, Eq. (4.14)], resulting in the sum of two hypergeomentric functions. Dissatisfied with this form, in [40] we proposed a change of functions and, using [30, Eq. 9.137.1], found two solutions distinguished by an inversion sign $\tau \in \{+, -\}$, each given by a single hypergeometric function:

$$\Psi^\kappa_{\lambda,\tau}(m) \;:=\; c^\kappa_\lambda\, \mathrm{i}^{\tau m}\, \frac{|\Gamma(\frac{1}{2}+\mathrm{i}\kappa+\tau m)|}{\Gamma(1-\mathrm{i}\lambda+\tau m)}\; {}_2F_1\left[\begin{matrix}\frac{1}{2}-\mathrm{i}\kappa-\mathrm{i}\lambda,\ \frac{1}{2}+\mathrm{i}\kappa-\mathrm{i}\lambda \\ 1-\mathrm{i}\lambda+\tau m\end{matrix}; \frac{1}{2}\right], \quad (6.14)$$

$$= \Psi^{-\kappa}_{\lambda,\tau}(m) = \Psi^\kappa_{\lambda,-\tau}(-m), \quad (6.15)$$

where c^κ_λ is an m-independent normalization coefficient that may be proposed from [20, Eq. (4.14)], but which for numerical purposes can be set to any constant value. When plotting these functions in Figure 6.3, we see that they are *the* right- and left-moving discrete repulsive oscillator wavefunctions [58, Fig. 7.11]) with energies $\eta = \lambda + \kappa$. The density plot of this basis in Figure 6.4 shows that the phase $\mathrm{i}^{\tau m}$ in (6.14) is indeed the appropriate one —otherwise the function would oscillate between neighboring positions. As for (5.6), we

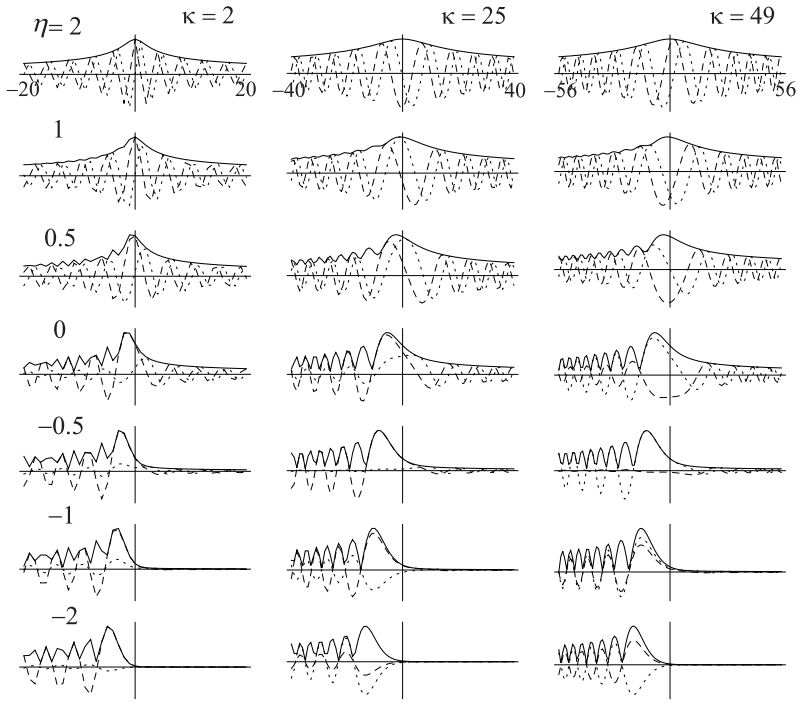

Figure 6.3: Discrete repulsive oscillator wavefunctions, $\Psi^{\kappa}_{\lambda,+}(m)$ in (6.14). The columns correspond to representations $\kappa = 2$, 25 and 49; the rows, to energies $\eta = \lambda + \kappa = 2$, 1, 0.5, 0, -0.5, -1, and -2. Dashed, dotted and continuous lines join the real, imaginary and absolute values of the functions between integer positions m, whose ranges are scaled by factors $\propto \sqrt{\kappa}$ attending to the contraction (6.16).

expect that

$$\lim_{\kappa\to\infty} \kappa^{1/4}\Psi^{\kappa}_{\lambda,\tau}(m) = \frac{\exp[\mathrm{i}\frac{1}{4}\pi(\frac{1}{2}-\mathrm{i}\eta)]}{2^{3/4}\pi}\Gamma(\tfrac{1}{2}-\mathrm{i}\eta)\, D_{-\frac{1}{2}+\mathrm{i}\eta}(\tau e^{\mathrm{i}3\pi/4}\sqrt{2}\,x), \qquad (6.16)$$

for $m = x\sqrt{\kappa}$ and $\eta = \lambda+\kappa$, should return the quantum wavefunctions with their parabolic cylinder functions $D_{\nu(z)}$.

As in previous cases, the discrete wavefunctions are actually analytic in the position coordinate m (set $\mathrm{i}^{\tau m} = \exp \mathrm{i}\frac{1}{2}\tau m$.), although in this case we could not factor them into a form with some known discrete special function. Regarding the asymptotic behavior $|m| \to \infty$, (6.13) shows that $\Psi^{\kappa}_{\lambda,\tau}(m+1) \approx -\Psi^{\kappa}_{\lambda,\tau}(m-1)$, so the chirp of the continuous case deforms into a highest frequency of period 4. Moreover, the use of (6.14) in numerical computations raises questions since it is a Dirac basis, so their norm is infinite. In Ref. [40] we commented on the use of N vectors $\Psi^{\kappa}_{\lambda_n,\tau}(m)$ of chosen λ_n's on N positions m, as a finite non-orthogonal basis.

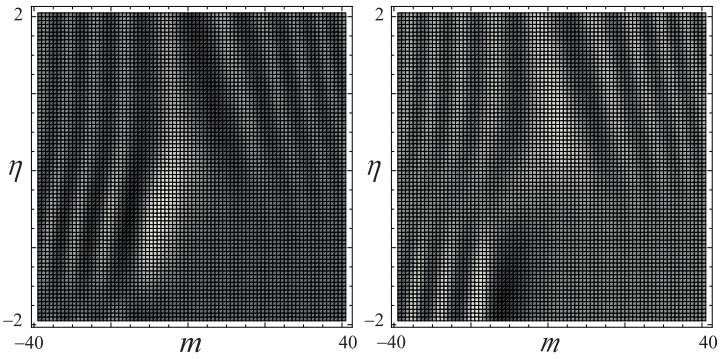

Figure 6.4: Density plots of the real (left) and imaginary (right) values of a (finite) discrete repulsive oscillator sub-basis $\Psi^{25}_{\lambda_i,+}(m)$ for 25 positions $m \in \{-12,-11,\ldots,12\}$, and 25 energies $\{\eta_i\}$ equally spaced between -2 and 2.

7 The iso(2) Free Case

The three-parameter Euclidean algebra iso(2) describes the discrete free particle, with $\sigma = 0$ in (3.7), on the infinite discrete position set of points $m \in \mathcal{Z}$. The spectrum $\{\lambda\}$ of $\mathcal{K}$ is evident when we realize the generators of the iso(2) algebra on the circle $\theta \in (-\pi,\pi]$, $\widehat{X} := -\mathrm{id}/\mathrm{d}\theta$, $\widehat{P} := l\sin\theta$ and $\widehat{K} = l\cos\theta$, so $\lambda = l\cos\theta$ and $-l \le \lambda \le l$, $l \in \mathsf{R}$. The eigenvalues of the Casimir operator are $\gamma = l^2$, and the recurrence relation (4.6) acquires a simple form when in (4.5) $c^{l^2}_{\updownarrow} = l$. We label the iso(2) representations with $l \ge 0$ and a dichotomic index υ,

$$l\,\Psi^l_{\lambda,\upsilon}(m{+}1) + 2\lambda\Psi^l_{\lambda,\upsilon}(m) + l\,\Psi^l_{\lambda,\upsilon}(m{-}1) = 0. \tag{7.1}$$

The two independent solutions, distinguished by υ as parity, are

$$\Psi^l_{\lambda,+}(m) = \frac{1}{\sqrt{\pi}}\cos(m\theta), \qquad \Psi^l_{\lambda,-}(m) = \frac{1}{\sqrt{\pi}}\sin(m\theta), \tag{7.2}$$

with $\theta = \arccos(\lambda/l)$, $\theta \in [0,\pi]$ and, according to (3.12), energy $\eta = \lambda{+}l = l(1{+}\cos\theta) \in [0,2l]$. In Figure 7.1 we show the free wavefunctions (7.2), noting that since they are analytic in m, we can plot them as if the functions were continuous.

The discrete free particle has thus a restricted continuous range of energies, bounded below by a constant wavefunction, and above by one with the shortest wavelength, whose period is 2. We may also use their complex linear combinations $\Psi^l_\lambda := (\Psi^l_{\lambda,+}{+}\mathrm{i}\Psi^l_{\lambda,-})/\sqrt{2}$ for $\theta \in (-\pi,\pi]$; thus in essence, the iso(2) basis (7.2) provides the Fourier series decomposition between bandlimited signals $f(\theta)$ and their Fourier coefficients f_m, which are interpreted as the discrete wavefunctions of a free system. The Euclidean case is well known in the model of an infinite discrete lattice of masses joined by springs, whose dynamics

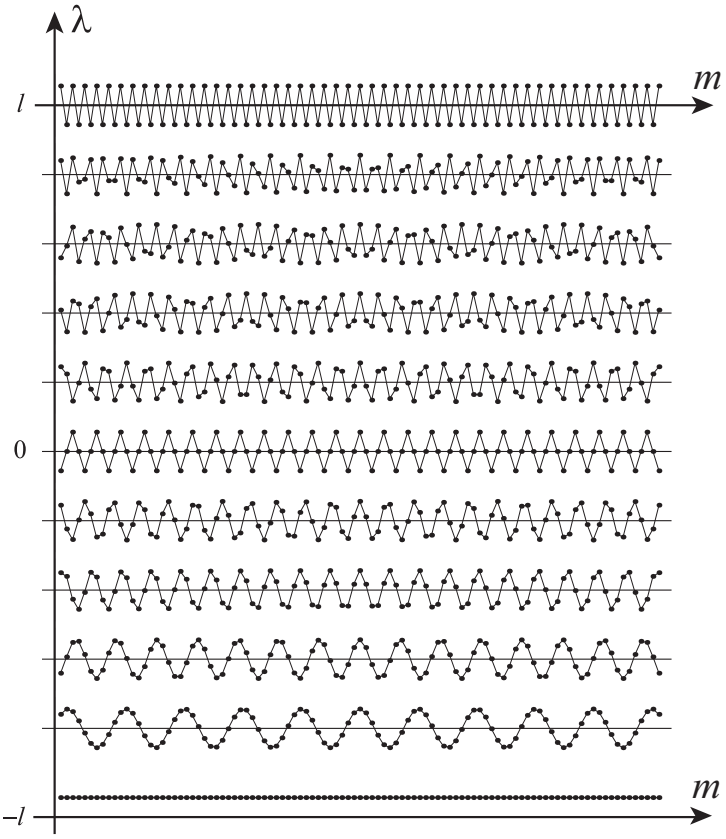

Figure 7.1: Discrete free particle wavefunctions, $\Psi^l_{\lambda,+}(m)$ and $\Psi^l_{\lambda,-}(m)$ in (7.2). Recall that $\lambda = l\cos\theta$, so that there is actually a continuum $-l \le \lambda \le l$ of energies $\eta = \lambda + l$; for $\theta = 0$ and π, $\Psi^l_{\pm l,-} = 0$.

is given by a Green function which is the bilinear generating function of the basis (7.2) integrated over the circle,

$$\begin{aligned} d^l_{m,m'}(\zeta) &:= (\Psi^l(m),\, \exp(-\mathrm{i}\zeta\mathcal{K})\,\Psi^l(m'))_{\mathcal{L}^2_{\mathcal{S}}} && (7.3)\\ &= \frac{1}{2\pi}\int_{-\pi}^{\pi} \mathrm{d}\theta\, \exp(-\mathrm{i}\zeta l\cos\theta)\, e^{\mathrm{i}(m'-m)\theta} \\ &= e^{\mathrm{i}\pi\,|m-m'|/2}\, J_{|m-m'|}(\zeta l). && (7.4)\end{aligned}$$

The Green matrices $\|d^l_{m,m'}(\zeta)\|$ are here symmetric, infinite circulating matrices, whose elements depend only on the distance $|m-m'|$ to the main diagonal. They exhibit the group property

$$\sum_{m'\in\mathcal{Z}} d^l_{m,m'}(\zeta_1)\, d^l_{m',m''}(\zeta_2) = d^l_{m,m'}(\zeta_1+\zeta_2). \qquad (7.5)$$

Indeed, the Green matrices belong to the irreducible representation l of a translation subgroup of the Euclidean group $\mathsf{ISO}(2)$, and correspond to the Wigner and Bargmann little-d's of rotations and boosts in the other two three-parameter groups. The same bilinear construction can be made for the other two cases to obtain the full representation matrices of the groups in 'Euler parametrization' as

$$D^s_{m,m'}(\alpha,\zeta,\gamma) = e^{-\mathrm{i}m\alpha}\, d^s_{m,m'}(\zeta)\, e^{-\mathrm{i}m'\gamma}, \tag{7.6}$$

where s stands for the j,k,l representation labels of the respective groups $\mathsf{SO}(3)$, $\mathsf{SO}(2,1)$ or $\mathsf{ISO}(2)$ used previously. Conversely, the signals $\Psi^s_\lambda(m)$ will transform linearly and irreducibly, as column vectors, under their irreducible representation matrices (7.6).

The wavefunctions $\Psi^s_\lambda(m)$ are orthonormal and complete, so any signal $f(m)$ can be decomposed into and synthesized from these *mode* coefficients. (We call them mode coefficients because for finite signals they provide the oscillator energy mode content.) Indicating by S the sum or integral over the range of pseudo-energies λ (the spectrum of $\mathcal{K}^{(\sigma)}$ in the representation s of the algebra), the analysis and synthesis of the signal in the mode basis is

$$f(m) = \mathop{\mathsf{S}}_{\lambda\in\Sigma(\mathcal{K},s)} f^s_\lambda\, \Psi^s_\lambda(m), \qquad f^s_\lambda = \sum_{x\in\Sigma(\mathcal{X},s)} f(m)\, \Psi^s_\lambda(m)^*, \tag{7.7}$$

with $\lambda(n)$ shifted appropriately. For $\mathsf{ISO}(2)$ this is the Fourier series decomposition, well-known and well applied. But when we return to our finite model of a parallel-processing optical chip in Figure 1.1, it is the finite case that should be of special interest, because considerable labor has been expended in using bases for (7.7) with sampled and orthonormalized Hermite-Gaussian functions [48, 49], Harper functions [19], and the non-orthogonal Mehta functions [34]. Comparing these sampled bases with the Kravchuk function basis (5.4), in Ref. [65] we addressed the questions of approximation and exact restoration of a signal when one has gained access only to a few of its lowest mode coefficients; in particular the concomitant finite Gibbs phenomenon at the sharp edges of rectangle signals. There are pros and cons in both bases.

8 Group Transformations and Aberrations

We turn now to extend the transformations due to the unitary action of the group elements of $\mathsf{SO}(3)$, $\mathsf{SO}(2,1)$ or $\mathsf{ISO}(2)$ on the finite or infinite signal vectors, and to introduce transformations outside those groups, which are also unitary, and which follow from the discrete quantization of the Lie-Hamilton aberrations in geometric optics [24,25,59]. Most of the work done so far has been for finite, N-point signals [64], *i.e.*, for $\mathsf{SO}(3)$. Certainly, as the optical model of Figure 1.1 suggests, the setup may not process the signal as a perfect harmonic oscillator, but may have aberrations [60]. In geometric optics [63, Part 4], these

aberrations are generated by nonlinear functions of the phase space coordinates x, p. For two-dimensional optics, we chose the basis of monomial power functions,

$$M^{r,\omega}(x,p) := p^{r+\omega}\, x^{r-\omega}, \tag{8.1}$$

of *weight* $\omega \in \{-k, -k+1, \ldots, k\}$, and of *rank* $r \in \{\frac{1}{2}, 1, \frac{3}{2}, \ldots\}$. Their Poisson operators $\{M^{r,\omega}, \circ\}$ act on the phase-space coordinates x, p turning them into monomial power functions of degree $A^c = 2r - 1$, that we call the classical aberration *order*. The one-parameter group of operators $\exp(\tau\{M^{r,\omega}, \circ\})$ thus acts *nonlinearly* in classical phase space. In Figure 8.1 we show these transformations.

Now we can **discretely quantize** the functions (8.1), here generalized to the three coordinates x, p, κ of the $\mathsf{so}(3)$ Lie algebra generators (2.6)–(2.8), which in the representation D^j of dimension $N = 2j + 1$ are the following matrices,

$$\begin{aligned}
\text{position} \qquad & x \leftrightarrow \mathbf{X} = \|X_{m,m'}\| \\
X_{m,m'} \;&=\; m\,\delta_{m,m'}, \qquad (8.2)\\
\text{momentum} \qquad & p \leftrightarrow \mathbf{P} = \|P_{m,m'}\| \\
P_{m,m'} \;&=\; -\mathrm{i}\tfrac{1}{2}\sqrt{(j-m)(j+m+1)}\,\delta_{m+1,\,m'} + \mathrm{i}\tfrac{1}{2}\sqrt{(j+m)(j-m+1)}\,\delta_{m-1,\,m'}, \qquad (8.3)\\
\text{(pseudo) energy} \qquad & h \leftrightarrow \mathbf{K} = \|K_{m,m'}\| \\
K_{m,m'} \;&=\; \tfrac{1}{2}\sqrt{(j-m)(j+m+1)}\,\delta_{m+1,\,m'} + \tfrac{1}{2}\sqrt{(j+m)(j-m+1)}\,\delta_{m-1,\,m'}. \qquad (8.4)
\end{aligned}$$

The position matrix $\mathbf{X}$ is diagonal, the matrix $\mathbf{K}$ is found replacing λ in (5.1), and $\mathbf{P}$ is obtained in the same way from (4.3), or from (2.9) by commuting $[\mathbf{K}, \mathbf{X}] = -\mathrm{i}\mathbf{P}$. The three matrices are hermitian and traceless; energy is represented by a real and symmetric matrix, while momentum is pure imaginary and skew-symmetric, as the Schrödinger operator $\widehat{P} = -\mathrm{i}\,\mathrm{d}/\mathrm{d}x$ is. The i-exponential of these matrices yields the representation j of the group $\mathsf{SO}(3)$, because their Casimir invariant is

$$\mathbf{X}^2 + \mathbf{P}^2 + \mathbf{K}^2 = j(j+1)\mathbf{1}. \tag{8.5}$$

Now, to introduce aberrations on the classical x, p, κ coordinates, we associate matrices to their monomials using the Weyl product rule:

$$\begin{aligned}
x^a p^b h^c \;&\leftrightarrow\; \{\mathbf{X}^a\,\mathbf{P}^b\,\mathbf{K}^c\}_{\text{Weyl}} \\
&:=\; \frac{1}{(a+b+c)!}\sum_{\text{permutations}} \overbrace{\mathbf{X}\cdots\mathbf{X}}^{a\text{ factors}}\,\overbrace{\mathbf{P}\cdots\mathbf{P}}^{b\text{ factors}}\,\overbrace{\mathbf{K}\cdots\mathbf{K}}^{c\text{ factors}}, \qquad (8.6)
\end{aligned}$$

and linear combination for summands. We note that a Weyl-ordered product of hermitian matrices is hermitian, and thus the matrices (8.6) will i-exponentiate to unitary ones. It

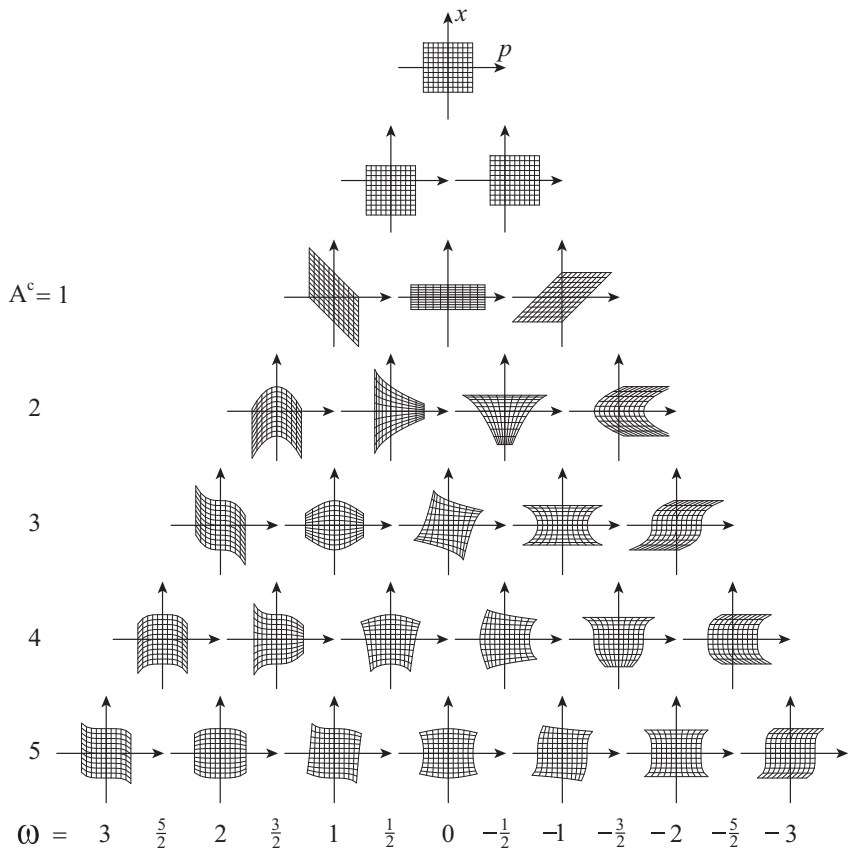

Figure 8.1: Infinite tower of linear transformations and aberrations of classical phase space x, p, generated by the monomials (8.1), classified by aberration order A and weight ω. The unit map is at the top; then come Heisenberg-Weyl translations along x and p (zero aberration order). The linear $\mathsf{Sp}(2,\mathsf{R})$ transformations ($A^{\rm c}=1$) are free propagation, (inverse) magnification, and a Fresnel lens. Higher aberrations of orders $A^{\rm c}=2,\ 3,\ 4,\ 5\ldots$ follow. In geometric optics, aligned systems produce only odd-order aberrations.

is not difficult to prove that through products and powers, the latter exhaust the full N^2-parameter Lie group $\mathsf{U}(N)$ of $N\times N$ unitary matrices. Of course, aberrations should not imply loss of signal information, so they should be represented by unitary matrices.

Since there cannot be more than N^2 independent $N\times N$ unitary matrices, the set of finite aberrations corresponding to (8.1) must contain redundancies. Equation (8.5) is one restriction that we choose to limit the powers of $\mathbf{K}$ to 0 or 1; and then we count the powers of $\mathbf{P}$ where the nonzero subdiagonals reach the matrix corners. In this way we can classify the generators of the $\mathsf{U}(N)$ aberration group following their classification in geometric

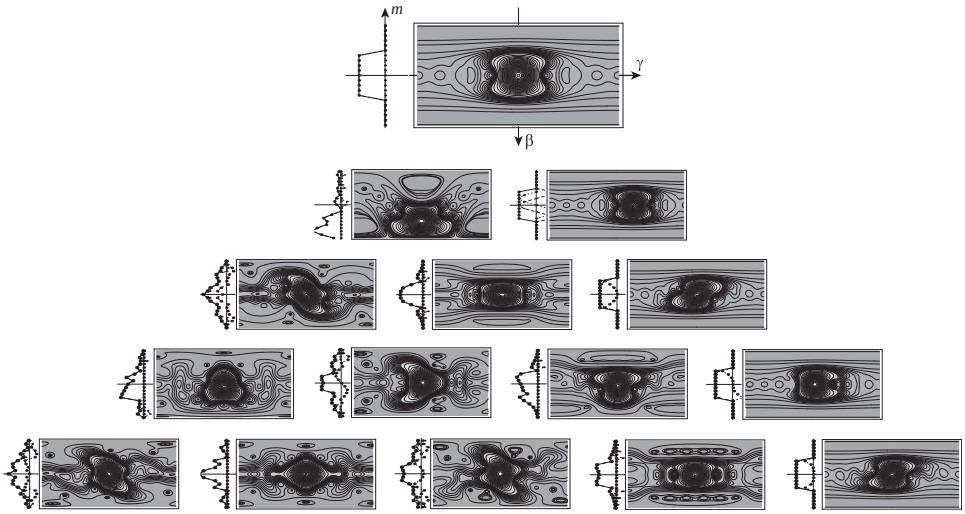

Figure 8.2: The first pyramid of aberrations up to order $A = 4$ for an $N = 21$-point signal. *Top*: Rectangle function shown left; at right, its Wigner function, projected on the (β, γ) polar coordinates of the sphere. *Second row*: $\mathsf{SO}(3)$-translations in position and momentum (aberration order $A = 1$) generated by $\mathbf{P}$ and $-\mathbf{X}$. *Following rows*: aberrations of orders 2, 3, and 4. The contour lines give higher resolutions to the near-zero values of the Wigner function: 0.0, ± 0.0001, ± 0.001, ± 0.01, 0.02, 0.03, ..., 0.15, 0.2, 0.3, ..., 3.0, 3.1.

optics, defining *two* pyramids of aberrations

$$\mathbf{M}^{r,\omega;0} := \{\mathbf{P}^{r+\omega}\mathbf{X}^{r-\omega}\}_{\text{Weyl}}, \qquad \omega \in \{-r, -r+1, \ldots, r\}, \tag{8.7}$$

$$\mathbf{M}^{r,\omega;1} := \{\mathbf{P}^{r-\frac{1}{2}+\omega}\mathbf{X}^{r-\frac{1}{2}-\omega}\mathbf{K}\}_{\text{Weyl}}, \quad \omega \in \{-r+\tfrac{1}{2}, -r+\tfrac{3}{2}, \ldots, r-\tfrac{1}{2}\}, \tag{8.8}$$

for integer $0 < A = 2r \leq N-1 = 2j$. It should be clear that we have handled these matrices through symbolic computation and numerical evaluation; the finite unitary matrices have then been produced through exponentiation. Although we have not defined yet what we are plotting, in Figures 8.2 and 8.3 we render the action of the single aberrations (8.7) and (8.8) on a map of the phase space of finite systems, to be compared with the classical deformations in Figure 8.1. In the Appendix we define the Wigner function for $\mathsf{SO}(3)$, its reduction to a sphere, and the projection of that sphere onto the $\pi \times 2\pi$ rectangles that appear in these figures. The signal that we exposed to aberrations is a rectangle function (top of Fig. 8.2). Overall phases are generated by $\mathbf{M}^{0,0,0} = \mathbf{1}$, followed by the $\mathsf{SO}(3)$-linear transformations generated by $\mathbf{M}^{1/2,-1/2,0} = \mathbf{X}$ and $\mathbf{M}^{1/2,1/2,0} = \mathbf{P}$ in the first pyramid. The second pyramid in Fig. 8.3 has on top the oscillator Hamiltonian $\mathbf{M}^{1/2,0,1} = \mathbf{K}$ that generates rotations of phase space. The rest are the first few of the $N^2 - 4$ aberrations.

For example, in the case of $N = 5$-point systems [64], $\mathsf{u}(5)$ has $5^2 = 25$ linearly independent generators. Four of these belong to the subgroup $\mathsf{u}(2)$: 1 for aberration order

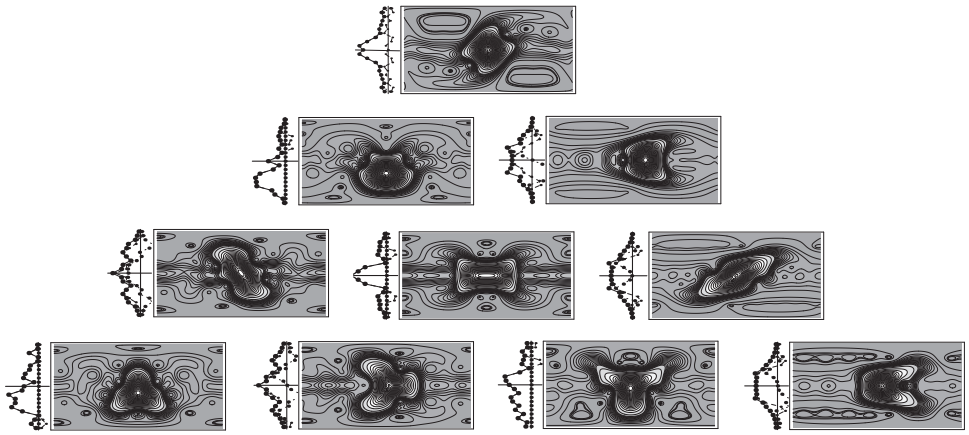

Figure 8.3: The second pyramid of aberrations up to order $A = 4$ for the same $N = 21$-point rectangle signal of the previous figure. *Top*: A 45° $\mathsf{SO}(3)$-linear rotation generated by $\mathbf{K}$, and its Wigner function (aberration order 1). *Following rows*: Aberrations of orders 2, 3 and 4. These are $\mathbf{K}$-repeaters of the aberrations of orders 1, 2, and 3 of the previous figure.

$A = 0$ of overall phases, and $A = 1$ for linear transformations. The rest are aberrations organized into two pyramids, for aberrations of orders $A = 2$, 3, and 4. They are the matrices obtained from the discrete quantization of x, p, κ as follows:

$$
\begin{array}{rccccccccc}
A^{k,\omega;0}(x,p)\text{:} & & & & & & & & & \\
A=0 & & & & & 1 & & & & k=0 \\
1 & & & & p & & x & & & \tfrac{1}{2} \\
2 & & & p^2 & & px & & x^2 & & 1 \\
3 & & p^3 & & p^2x & & px^2 & & x^3 & \tfrac{3}{2} \\
4 & p^4 & & p^3x & & p^2x^2 & & px^3 & & x^4 \quad 2 \\
\omega = & 2 & \tfrac{3}{2} & 1 & \tfrac{1}{2} & 0 & -\tfrac{1}{2} & -1 & -\tfrac{3}{2} & -2,
\end{array}
\tag{8.9}
$$

$$
\begin{array}{rccccccc}
A^{k,\omega;1}(x,p,\kappa)\text{:} & & & & & & & \\
A=1 & & & & \kappa & & & k=\tfrac{1}{2} \\
2 & & & \kappa p & & \kappa x & & 1 \\
3 & & \kappa p^2 & & \kappa px & & \kappa x^2 & \tfrac{3}{2} \\
4 & \kappa p^3 & & \kappa p^2 x & & \kappa px^2 & & \kappa x^3 \quad 2 \\
\omega = & \tfrac{3}{2} & 1 & \tfrac{1}{2} & 0 & -\tfrac{1}{2} & -1 & -\tfrac{3}{2}.
\end{array}
\tag{8.10}
$$

There are 15 entries in the first pyramid and 10 in the second, summing up to the 25 generators of $\mathsf{u}(5)$.

To write the unitary matrix that represents a given geometric optical setup as a finite system, we recall [63, Part 4] that the classical, nonlinear canonical transformation

is parametrized by the aberration coefficients $\mathbf{A} = \{A^r\} = \{\{A^{r,\omega}\}\}$ of its *factored-order* product form [24],

$$\mathcal{G}(\mathbf{A}, S) := \cdots \exp\{G_2(A_2), \circ\} \exp\{G_{3/2}(A_{3/2}, \circ\} \exp\{G_1(A_1), \circ\}, \quad (8.11)$$

$$G_r(A_r)(x,p) := \sum_{\omega=-r}^{r} A_{r,\omega}\, M^{r,\omega}(x,p). \quad (8.12)$$

The rightmost factor in (8.11) is an $\mathsf{Sp}(2,\mathsf{R})$-linear transformation, and to its left, transformations of increasing aberration order. These classical operators can be concatenated; the composition rule for the aberration coefficients of the product in terms of the factors has been computed to odd aberration orders up to seven [25], [63, Sect. 14.4]. For free flight, refracting interfaces, and anharmonic waveguides, the aberration coefficients $A_{r,\omega}$ are given in [63, Sect. 14.5] up to that order. The finite matrix analogue to the above construction can be reproduced forthwith, leading to a factored-product parametrization of the elements of the unitary groups $\mathsf{U}(N)$, $N = 2j+1$, by $\mathbf{A} = \{\mathbf{A}_r\}_{r=0}^{2j}$, $\mathbf{A}_r = \{A_{r,\omega}\}_{\omega=-r}^{r}$, as

$$\begin{aligned} \mathbf{U}_N(\mathbf{A}) &= \mathbf{U}_{N-1}(\mathbf{A}_{N-1}) \times \mathbf{U}_{N-2}(\mathbf{A}_{N-2}) \times \\ &\qquad \cdots \times \mathbf{U}_2(\mathbf{A}_2) \times \mathbf{U}_1(\mathbf{A}_1), \quad (8.13) \\ \mathbf{U}_r(\mathbf{A}_r) &:= \exp\Big[-\mathrm{i}\Big(\sum_{\omega=-r}^{r} A_{r,\omega;0}\mathbf{M}^{r,\omega;0} + \sum_{\omega=-r}^{r} A_{r,\omega;1}\mathbf{M}^{r,\omega;1}\Big)\Big], \quad (8.14) \end{aligned}$$

where the rightmost factor in (8.13) is the $N \times N$ matrix representation of $\mathsf{SO}(3)$.

Although the commutators of Poisson operators and of matrices are different due to the nonstandard commutator in the latter, it seems to us that the performance of a complete optical setup can be translated identifying only $A^{r,\omega} \leftrightarrow A_{r,\omega;0}$. The reason for this, as will be borne out in the Appendix, is that the transformation of phase space in the finite system, which is a sphere whose low-energy pole is tangent to the origin of classical phase space, the two neighborhoods flow in the same way under the exponentiated Poisson operator, as under the $\mathbf{M}^{r,\omega;0}$'s and the $\mathbf{M}^{r,\omega;1}$'s (see Fig. 10.1); at the top pole, the last two flow in opposite directions. It would seem that the coefficients of the aberrations $\mathbf{M}^{r,\omega;1}$ of the second pyramid can be taken proportional to the coefficients of the first. This point requires further research and concrete optical setup examples with sampled wavefields.

9 Two-Dimensional Discrete Systems

With an eye on applications to image processing, we have investigated the two-dimensional case, where the discrete image wavefunctions can be sensed (with complex values) or seen on pixellated screens. There has been an upsurge of interest in producing laser beams whose transverse sections exhibit nodes along lines, circles and radii, ellipses

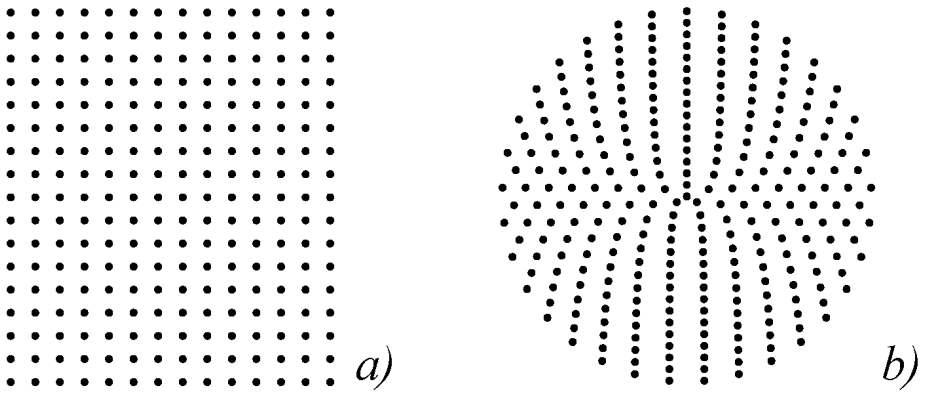

Figure 9.1: Two-dimensional screens pixellated screens for $j = 8$. *(a)*: Cartesian arrangement $(m_1,\, m_2)$ of the 17^2 sensor points. *(b)*: Polar arrangement $(\rho,\, \phi_k)$ of the same number of points, on circles of integer radii $\rho \in [0, 2j]$ and, on each circle, $2\rho{+}1$ equidistant points ϕ_k.

and hyperbolas, and parabolas [17]. The question to be raised is whether a discrete and finite version of these geometries can be conjured, *i.e.*, separated in Cartesian, polar, elliptic or parabolic discrete variables. Thus with a circular array of CCD sensors one could test the quality of Bessel-Gauss beams, and probably do so better than with the Cartesian arrays currently used. Since $\mathsf{SO}(3)$ mothered finite Hamiltonian 1-dim systems, we proposed $\mathsf{SO}(4)$ to nurture 2-dim ones. The $\mathsf{so}(4)$ algebra of this group has the remarkable accidental property of being a direct sum of two $\mathsf{so}(3)$'s, and thus it has two nonequivalent subalgebra chains:

$$\mathsf{so}(2)_a \oplus \mathsf{so}(2)_b \subset \mathsf{so}(3)_a \oplus \mathsf{so}(3)_b \equiv \mathsf{so}(4) \supset \mathsf{so}(3)_{\rm x} \supset \mathsf{so}(2)_\mu, \tag{9.1}$$

where the spectra of the generators of $\mathsf{so}(2)_a$ and $\mathsf{so}(2)_b$ are the discrete Cartesian coordinates $m_1,\, m_2 \in [-j, j]$, while the generators of $\mathsf{so}(3)_{\rm x}$ will have spectra describing discrete polar coordinates, with $\mathsf{so}(2)_\mu$ playing the role of angular momentum operator. The two pixellations are shown in Figure 9.1. The details of this construction have appeared in several places [10–13] so here we shall only provide a review illustrated with some results.

9.1 The Cartesian-pixellated screen

We define Cartesian pixellation through the eigenvalues of operators in the direct sum of two mutually commuting algebras,

$$\mathsf{so}(3)_1 := \text{span}\,\{\mathcal{X}_1, \mathcal{P}_1, \mathcal{K}_1\}, \qquad \mathsf{so}(3)_2 := \text{span}\,\{\mathcal{X}_2, \mathcal{P}_2, \mathcal{K}_2\}, \tag{9.2}$$

in representations j_1 and j_2 respectively, in the terms of Section 5. We construct the position-Kronecker basis as eigenbasis of $\mathcal{X}_1$, $\mathcal{X}_2$ as in (3.3), and label the vectors by

$f^{j_1,j_2}_{m_1,m_2}$, with $-j_i \le m_i \le j_i$, $i = 1, 2$. We regard (m_1, m_2) as the discrete coordinates of a rectangular array of $N_1 \times N_2$ points, $N_i = 2j_i + 1$. Next, the mode eigenbasis of the pseudo-energy operators $\mathcal{K}_1$, $\mathcal{K}_2$, as in (4.1) will be indicated $h^{j_1,j_2}_{n_1,n_2}$, labelled by their mode numbers $n_i = \lambda_i + j_i \in [0, 2j_i]$. A 'pixellated image' $\mathbf{F}$ thus consists of the matrix of values $F_{m_1,m_2} = (f^{j_1,j_2}_{m_1,m_2}, \mathbf{F})$, and its mode content will be $\widetilde{F}_{n_1,n_2} = (h^{j_1,j_2}_{n_1,n_2}, \mathbf{F})$; the two sets of coordinates are related by the overlap functions

$$\Psi^{j_1,j_2}_{n_1,n_2}(m_1, m_2) := (f^{j_1,j_2}_{m_1,m_2},\, h^{j_1,j_2}_{n_1,n_2}), \tag{9.3}$$

which are given by a product of two $\Psi^j_n(m)$ functions (5.4), in m_1 and m_2. These are the Cartesian modes of a finite oscillator with total *mode* $n := n_1 + n_2 \in [0, 2j_1 + 2j_2]$ (energy $n + 1$), and energy *difference* $\mu = \frac{1}{2}(n_1 - n_2)$. In Figure 9.2*a* we show the finite Cartesian oscillator modes for the case of a square screen $j_1 = j_2$, arranged in a rhombus $(n, \mu) \in \diamond$ according to total mode number n (vertical) and difference μ (horizontal). These are the finite analogues of the Hermite-Gauss 2-dim beams in wave optics.

The continuous 2-dim quantum harmonic oscillator —and the free wave equation— separate in Cartesian and polar (and elliptic) coordinates of the plane; Laguerre-Gauss beams have nodes that fall on circles and radii, and are obtained by a $\frac{1}{2}\pi$ *gyration* within the $\mathsf{U}(2)$ group of 2-dim-Fourier transforms [51]. We *import* [10, 67] this transformation onto the finite $N_1 \times N_2$ screen with the same linear combination coefficients that involve a Wigner little-d function and provide the transform and its inverse, [26, Chap. 1],

$$\Lambda^{j_1,j_2}_{n,\mu}(m_1, m_2) := \sum_{n_1+n_2=n} e^{\mathrm{i}(n_1-n_2)/4}\, d^{n/2}_{\mu/2,\,(n_1-n_2)/2}(\tfrac{1}{2}\pi)\, \Psi^{j_1,j_2}_{n_1,n_2}(m_1, m_2), \tag{9.4}$$

$$\Psi^{j_1,j_2}_{n_1,n_2}(m_1, m_2) = \sum_{\mu=-n}^{n} e^{-\mathrm{i}(n_1-n_2)/4}\, d^{n/2}_{\mu/2,\,(n_1-n_2)/2}(\tfrac{1}{2}\pi)\, \Lambda^{j_1,j_2}_{n,\mu}(m_1, m_2). \tag{9.5}$$

This is a unitary transformation between two orthonormal bases (it is *not* within $\mathsf{so}(3)_1 \oplus \mathsf{so}(3)_2$ however), which defines the 'Laguerre-Kravchuk' finite basis shown in Figure 9.2*b*, also arranged in a rhombus (n, μ) for $j_1 = j_2$ (when $j_1 \neq j_2$ the arrangement yields a $45°$-rotated rectangle). We can call μ the *angular momentum* label for the wavefield, which visibly corresponds to its role in wavefield physics; yet it should be clear that it is *not* the eigenvalue of any operator in $\mathsf{so}(3)_1 \oplus \mathsf{so}(3)_2$. Still, on the basis (9.4) of energy and angular momentum, we define the operation of *rotation* of these modes by angles α, quite naturally as multiplication by a phase,

$$\mathcal{R}(\alpha)\, \Lambda^{j_1,j_2}_{n,\mu}(m_1, m_2) := \exp(-\mathrm{i}\mu\alpha)\, \Lambda^{j_1,j_2}_{n,\mu}(m_1, m_2). \tag{9.6}$$

With these tools we can rotate Cartesian-pixellated images $\mathbf{F} = \{F_{m_1,m_2}\}$, expanding first its coordinates in the (n, μ) basis, then multiplying them by $\exp(-\mathrm{i}\mu\pi)$, and then expanding back in that basis,

$$F^{(\alpha)}_{m_1,m_2} \quad = \quad \sum_{m'_1,m'_2} R_{m_1,m_2,\,m'_1,m'_2}\, F_{m'_1,m'_2}, \tag{9.7}$$

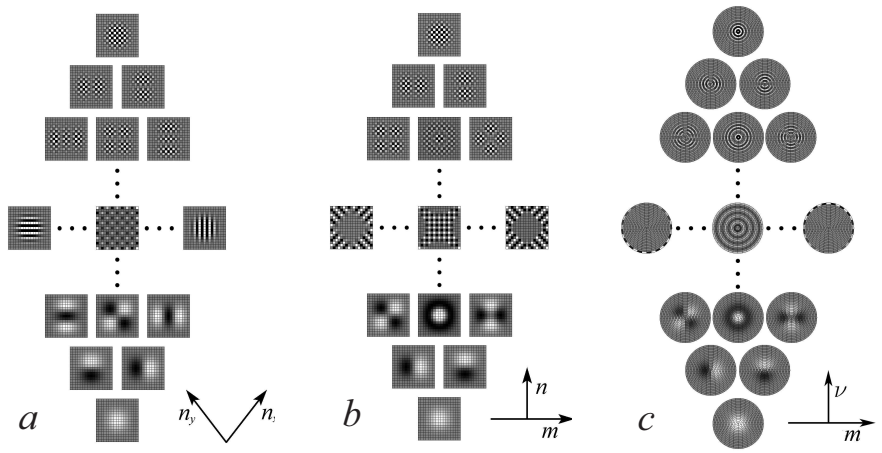

Figure 9.2: Two-dimensional modes on pixellated screens. *(a)*: Cartesian eigenmodes $\Psi^{j,j}_{n_1,n_2}(m_1,m_2)$ given the the product of two $\Psi^j_n(m)$ functions (5.4) on the Cartesian grid $m_1,\ m_2$, arranged according to their mode numbers $n_1,\ n_2$ (diagonal); the ground state is at bottom and the highest at top. *(b)*: Angular momentum modes on the Cartesian grid, $\Lambda^{j,j}_{n,\mu}(m_1,m_2)$ given by (9.4), arranged according to radial mode n (vertical) and angular momentum μ. *(c)*: Angular momentum modes on the polar grid, $\Psi^j_{n,\mu}(\rho,\phi_k)$ in (9.20) *et seq.*, also arranged by $n,\ \mu$; the left and right corners of the rhombus correspond to states with the highest possible angular momenta, which are concentrated on the rim of the screen.

$$R_{m_1,m_2,\,m_1',m_2'} \quad := \quad \sum_{n,\mu} \Lambda^{j_1,j_2}_{n,\mu}(m_1,m_2)e^{-\mathrm{i}\mu\alpha}\Lambda^{j_1,j_2}_{n,\mu}(m_1',m_2')^*. \tag{9.8}$$

In Figure 9.3 we show the effect of rotations of a 'black-and-white' image. Aliasing occurs at sharp edges that are not aligned with the axes (this is *not* a Gibbs phenomenon because the basis is complete); slightly smoothing the image edges quickly dampens the alias. The implementation of this algorithm and its graphical representations were the subject of the Ph.D. thesis of Dr. Luis Edgar Vicent. Commercial image-rotation algorithms simply interpolate new pixel values from a small neighborhood of the old, and consecutive rotations would degrade the image (which of course is kept in memory). By contrast, our rotations form a one-parameter unitary group; they are exact, multiplicative and reversible —but therefore 'slow,' *i.e.*, processing $N \times N$ images involves $\sim N^4$ multiplications and sums. Yet we may assume that if a paraxial optical rotator device is built [63, Sect. 10.2.3], it will perform (9.7)–(9.8) in parallel.

9.2 The polar-pixellated screen

We shall now set up two-dimensional finite Hamiltonian systems, as if *ab initio*, following the line of reasoning of Section 2, but introducing angular momentum among the

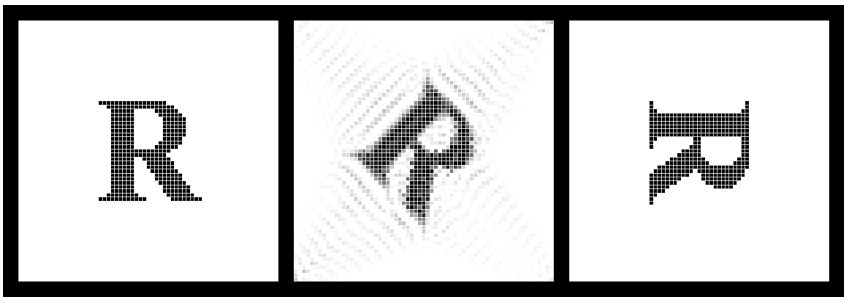

Figure 9.3: Rotation of a two-dimensional pixellated image on a Cartesian screen, using the algorithm (9.7)–(9.8), by 0°, 45°, and 90°.

Hamilton equations of an isotropic harmonic oscillator. Thus, we call into existence two position operators $\mathcal{X}_1,\ \mathcal{X}_2$, and a (single) Hamiltonian pseudo-energy operator $\mathcal{K}$; by commutation we define the two momenta $\mathcal{P}_i := \mathrm{i}[\mathcal{K}, \mathcal{X}_i]$, $i = 1,\ 2$. The classical Poisson-bracket relations for angular momentum are straightforwardly translated to the commutators of an operator $\mathcal{M}$, as

$$\begin{array}{ll} [\mathcal{M}, \mathcal{X}_1] = +\mathrm{i}\mathcal{X}_2, & [\mathcal{M}, \mathcal{P}_1] = +\mathrm{i}\mathcal{P}_2, \\ [\mathcal{M}, \mathcal{X}_2] = -\mathrm{i}\mathcal{X}_1, & [\mathcal{M}, \mathcal{P}_2] = -\mathrm{i}\mathcal{P}_1, \end{array} \quad [\mathcal{M}, \mathcal{K}] = 0. \tag{9.9}$$

To have a discrete Hamiltonian system, we deform the Heisenberg commutators ($[\mathcal{X}_i, \mathcal{P}_j] = \mathrm{i}\mathit{1}$, $[\mathcal{X}_i, \mathcal{X}_j] = 0$, and $[\mathcal{P}_i, \mathcal{P}_j] = 0$), replacing them with

$$[\mathcal{X}_1,\ \mathcal{P}_1\,] \;=\; \mathrm{i}\sigma\mathcal{K} = [\mathcal{X}_2, \mathcal{P}_2], \tag{9.10}$$

$$[\mathcal{X}_1,\ \mathcal{X}_2] \;=\; \mathrm{i}\,\mathcal{M} = [\mathcal{P}_1, \mathcal{P}_2], \tag{9.11}$$

$$[\mathcal{X}_1,\ \mathcal{P}_2] \;=\; 0 \;=\; [\mathcal{X}_2, \mathcal{P}_1], \tag{9.12}$$

where σ allows us to have a three-fold choice of algebras, as in Section 2. For the 2-dim harmonic oscillator $\sigma = +1$, the six operators $\{\vec{\mathcal{X}},\ \vec{\mathcal{P}},\ \mathcal{K},\ \mathcal{M}\}$ close into the four-dimensional rotation Lie algebra $\mathsf{so}(4)$; for $\sigma = -1$ it is the Lorentz algebra $\mathsf{so}(3,1)$, while for $\sigma = 0$ one has the 3-dim Euclidean algebra $\mathsf{iso}(3)$. The latter two algebras will provide *infinite* 2-dim pixellated screens, which are not of our concern at present.

We should have two commuting operators to determine simultaneously the radius and the angle coordinates of a pixel, both discrete and finite. The values of a signal at a finite number of angles on a circle $\{\phi_k\}$, subject to ordinary finite Fourier transformation, yield the same finite number of conjugate angular momentum values $\{\mu_k\}$; we should thus search for a *radial*-coordinate operator, yielding eigenvalues ρ (or ρ^2), among those that conmute with the $\mathcal{M}$, the angular momentum generator. The two will then provide a Kronecker basis for discrete polar coordinates, on which to put the pixels of the screen. And then, we shall build the energy-momentum eigenbasis where the commuting $\mathcal{K}$ and $\mathcal{M}$ are diagonal.

To organize the generators of the $\mathsf{so}(4)$ algebra, we write them as $\mathcal{L}_{i,j} = -\mathcal{L}_{j,i}$ in the following pattern:

$$\begin{array}{|c|c|c|}\hline \mathcal{L}_{1,2} & \mathcal{L}_{1,3} & \mathcal{L}_{1,4} \\ \hline \bullet & \mathcal{L}_{2,3} & \mathcal{L}_{2,4} \\ \cline{2-3} & \bullet & \mathcal{L}_{3,4} \\ \cline{2-3}\end{array} \quad := \quad \begin{array}{|c|c|c|}\hline \mathcal{K} & \mathcal{P}_1 & \mathcal{P}_2 \\ \hline \bullet & \mathcal{X}_1 & \mathcal{X}_2 \\ \cline{2-3} & \bullet & \mathcal{M} \\ \cline{2-3}\end{array} \,. \tag{9.13}$$

In this pattern, a generator $\mathcal{L}_{i,j}$ has *non*-zero commutator with those in its row i or its column j (reflecting these lines at the •'s); with all others the commutator is zero. Thus at a glance we can identify in (9.13) some subalgebra chains of $\mathsf{so}(4)$, in particular for $\mathsf{SO}(3)_{\rm x}$ in (9.1),

$$\mathsf{so}(3)_{\rm x} := \text{span}\,\{\mathcal{X}_1, \mathcal{X}_2, \mathcal{M}\} \supset \mathsf{so}(2)_\mu := \text{span}\,\{\mathcal{M}\}. \tag{9.14}$$

We recall that the $\mathsf{so}(4)$ algebra has two Casimir operators, $\mathcal{C}_1 = \sum_{i<j} \mathcal{L}_{i,j}\mathcal{L}_{i,j}$ and $\mathcal{C}_1 = \sum_{i<j,k} \mathcal{L}_{i,j}\mathcal{L}_{k,4}$, which are the sum and difference respectively of the Casimir operators of the two subalgebras $\mathsf{so}(3)_a \oplus \mathsf{so}(3)_b$ in (9.1), $j_a(j_a{+}1)$ and $j_b(j_b{+}1)$; when $j_a = j_b$ ('square' representation), the second is zero. Also, we recall that in the Gel'fand-Tsetlin canonical chain $\mathsf{so}(4) \supset \mathsf{so}(3) \supset \mathsf{so}(2)$ [28], the representation (j_a, j_b) contains the representations $|j_a{-}j_b| \le \ell \le j_a{+}j_b$ of $\mathsf{so}(3)$; and each of these, representations $\mu \in \{-\ell, \ldots, \ell\}$ of $\mathsf{so}(2)$. Thus, if we want the array to have a pixel at its center (no angle, thus $\mu = 0 = j$) then we must consider only square representations (j, j) of $\mathsf{so}(4)$. (We have not analyzed annular pixellated screens yet, but I assume it can be done.) Hence, when we diagonalize the Casimir operator of $\mathsf{so}(3)_{\rm x}$ in (9.14), it becomes

$$\mathcal{C}_X := \mathcal{X}_1^2 + \mathcal{X}_2^2 + \mathcal{M}^2 = \rho(\rho{+}1)\mathit{1}, \quad \rho \in \{0,\, 1,\, \ldots, 2j\}, \tag{9.15}$$

and each eigenvalue ρ reduces to the eigenvalues $-\rho \le \mu \le \rho$ of $\mathcal{M}$. There is thus a total of $\sum_{\rho=0}^{2j}(2\rho{+}1) = N^2$ distinct points (ρ, μ) for $N = 2j{+}1$, that we identify as the coordinates of discrete radius and angular momentum. Let us label the eigenbasis vectors of $\mathcal{C}_X$ and $\mathcal{M}$ by $\widetilde{f}^j_{\rho,\mu}$; then, the Kronecker eigenbasis for a polar array of points will be

$$f^j_{\rho,\phi_k} := \frac{1}{\sqrt{N}} \sum_{\mu=-\rho}^{\rho} \exp(\mathrm{i}\mu\phi_k)\, \widetilde{f}^j_{\rho,\mu}, \qquad \begin{array}{c}\phi_k := 2\pi k/(2\rho{+}1), \\ -\rho \le k \le \rho.\end{array} \tag{9.16}$$

The sensor points will thus be arranged in circles of radii $\rho \in \{0, 1, 2, \ldots, 2j\}$, and on each of them there will be $1, 3, 5, \ldots, 2\rho{+}1, \ldots, 4j{+}1$ points.

On the other hand, for the eigenbasis of energy and angular momentum, where $\mathcal{K}$, $\mathcal{M}$ have eigenvalues $-j \le \lambda, \mu \le j$, we have the information that they appear in the direct sum $\mathsf{so}(3)_a \oplus \mathsf{so}(3)_b \equiv \mathsf{so}(4)$ of the algebras [29, 63, p. 241],

$$\mathsf{so}(3)_a \;\; := \;\; \text{span}\,\{\tfrac{1}{2}(\mathcal{X}_1{+}\mathcal{P}_2),\, \tfrac{1}{2}(\mathcal{X}_2{-}\mathcal{P}_2),\, \tfrac{1}{2}(\mathcal{K}{+}\mathcal{M})\}, \tag{9.17}$$

$$\mathsf{so}(3)_b \;:=\; \text{span}\,\{\tfrac{1}{2}(\mathcal{X}_1{-}\mathcal{P}_2), -\tfrac{1}{2}(\mathcal{X}_2{+}\mathcal{P}_2),\, \tfrac{1}{2}(\mathcal{K}{-}\mathcal{M})\}, \tag{9.18}$$

The labels (λ,μ) within $\mathsf{so}(2)_a \oplus \mathsf{so}(2)_b$ will thus organize themselves into a rhombus $\diamond$, exactly as for $\Lambda^{j,j}_{n,\mu}$ in (9.4), with $n = \lambda{+}j$. Thus we have defined the energy eigenbasis $h^{j,j}_{\lambda,\mu}$.

Now, as the third step, we must find the actual polar-pixellated eigenfunctions of angular momentum and energy, as the overlap (9.16) [*cf.* (4.2), (6.6) and (9.3)],

$$\Psi^j_{n,\mu}(\rho,\phi_k) \;:=\; (f^j_{\rho,\phi_k},\, h^{j,j}_{\lambda,\mu}) \qquad n=\lambda{+}j \tag{9.19}$$

$$\;=\; \frac{1}{\sqrt{N}} \sum_{\mu=-\rho}^{\rho} \exp(-\mathrm{i}\mu\phi_k)\, \Lambda^j_\lambda(\rho,\mu), \qquad \phi_k = \frac{2\pi k}{2\rho{+}1}, \tag{9.20}$$

$$\Lambda^j_\lambda(\rho,\mu) \;:=\; (\widetilde{f}^j_{\rho,\mu}, h^{j,j}_{\lambda,\mu}). \tag{9.21}$$

All ϕ_k-dependence is in the exponentials $\exp(-\mathrm{i}\mu\phi_k)$, which multiply the *radial* discrete oscillator wavefunctions $\Lambda^j_\lambda(\rho,\mu)$ in (9.20), so we have achieved a separation of discrete polar coordinates. The evaluation of the last overlap is actually the Clebsch-Gordan problem of coupling the two quantum angular momenta $j,\, j$ in $\mathsf{so}(3)_a \oplus \mathsf{so}(3)_b$ to the angular momentum ρ (which here has the meaning of radius!); the row labels of $\mathsf{so}(2)_a \oplus \mathsf{so}(2)_b$ in (9.17)–(9.18) are $\frac{1}{2}(\lambda{+}\mu)$ and $\frac{1}{2}(\lambda{-}\mu)$, so that

$$\Lambda^j_\lambda(\rho,\mu) = \varphi(j,\rho,\lambda,\mu) \begin{pmatrix} j, & j; & \rho \\ \frac{1}{2}(\mu{+}\lambda), & \frac{1}{2}(\mu{-}\lambda); & \mu \end{pmatrix}, \tag{9.22}$$

where $\begin{pmatrix} j_1, & j_2, & j \\ m_1, & m_2, & m \end{pmatrix}$ is the Clebsch-Gordan coefficient, and there is a sign phase [11, 54],

$$\varphi(j,\rho,\lambda,\mu) := (-1)^{j+\rho+\frac{1}{2}(|m|-m)} \exp(\mathrm{i}\tfrac{1}{2}\pi\lambda), \tag{9.23}$$

due to the fact that the Gel'fand-Tsetlin chain $\mathsf{so}(4) \supset \mathsf{so}(3)$ involves the subalgebra $\{\mathcal{L}_{i,j}\}^3_{i,j=1}$, while in (9.13) we used the subalgebra $\{\mathcal{L}_{i,j}\}^4_{i,j=2}$. The wavefunctions are orthonormal and complete with respect to the discrete variable pairs (ρ,ϕ_k), (ρ,μ) and (λ,μ) or (n,μ).

Clebsch-Gordan coefficients can be written in several ways, including a form with a factor that has no zeros on $\rho \in [0, 2j]$, and a ${}_3F_2$-hypergeometric function of unit argument, which is a *dual-Hahn* polynomial of degree $n = \lambda{+}j$ in $\rho(\rho{+}1)$. In Figure 9.2*c* we show the real part of the polar-pixellated wavefunctions $\Psi^j_{n,\mu}(\rho,\phi_k)$ in (9.19). Note that due to the rhombus relation between $n = \lambda{+}j$ and $|\lambda{\pm}\mu| \le j$, these functions are zero for radii $\rho < |\mu|$; this seems to be the counterpart to the multiple zeros at the origin exhibited by the continuous radial-separated oscillator wavefunctions. Finally, in the $j \to \infty$ limit, the $\Psi^j_{n,\mu}(\rho,\phi_k)$'s converge to the continuous Laguerre-Gauss functions [13].

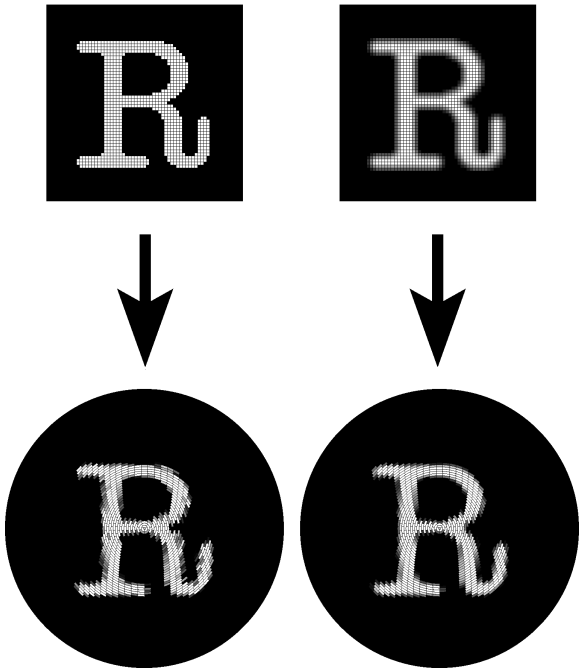

Figure 9.4: Map between a pixellated image on a Cartesian screen (left), to an image pixellated on a polar screen by the algorithm (9.24)–(9.25).

9.3 Mapping square ↔ polar screens

As promised at the beginning of this Section, we can now map pixellated images $\mathbf{F}$ between Cartesian and polar geometries. The key is to identify the eigenfunctions of energy and angular momentum in each of the previous subsections, *i.e.*, $\Lambda^{j,j}_{n,\mu}(m_1,m_2)$ in (9.4) and $\Psi^j_{n,\mu}(\rho,\phi_k)$ in (9.20)–(9.23). If an image $\mathbf{F}$ in a square-pixellated screen is $\{F(m_1,m_2)\}$, (m_1,m_2), $m_i\in[-j,j]$, then its unitary transfer to a polar-pixellated screen (ρ,ϕ_k), $\rho\in[0,2j]$, $k\in[-\rho,\rho]$ will be

$$F_\circ(\rho,\theta_k) \;=\; \sum_{m_1,m_2=-j}^{j} U^j(\rho,\theta_k;\,m_1,m_2)\,F(m_1,m_2), \qquad (9.24)$$

$$U^j(\rho,\theta_k;\,m_1,m_2) \;:=\; \sum_{n,\mu\in\diamondsuit} \Psi^j_{n,\mu}(\rho,\phi_k)\,\Lambda^{j,j}_{n,\mu}(m_1,m_2)^*, \qquad (9.25)$$

where the transform kernel is obtained by summing n,m over their values in the rhombi of Figure 9.2*a–c*. In Figure 9.4 we show an example of this map from the Ph.D. Thesis of Dr. Luis Edgar Vicent [52].

10 Conclusions

The theory of Lie algebras and groups contains structures that describe select continuous and discrete Hamiltonian systems. These structures led to results and insights in mathematics, including the theory of separation of variables and special functions [35], phase space distribution functions in quantum mechanics [33, 55], geometric and quantum optics [50, 63], and quantum computing —whose wide literature is better known to the participants of the 2009 Sohag conference than to this author.

As is often the case in mathematical physics, we may be offering solutions to problems not yet formulated. In this essay we recounted and referenced the topics presented at the Conference, on one- and two-dimensional 'toy' models in geometric and laser-beam optics, and in mechanics. Other lines of research that we have not mentioned include the use of the (non-Lie) q-algebra $\mathsf{su}(2)_q$ to describe discrete models where the sensor positions are not equally spaced but crowd towards the center, and phase space is a revolution spheroïd [7,8].

The phase space description of infinite discrete signals within $\mathsf{so}(2,1)$ representations was not been reported here because it is not yet complete. Particularly, we are curious about the location of three geometric-optical fractional Fourier transformers with lens- and mirror-arrangements [63, Chap. 15] within the group $\mathsf{U}(N)$ of $\mathsf{SO}(3)$ systems [31] with aberrations, and their comparison in experimental setups; for vector signals, density matrices, or 2-dim finite pixellated images. One particularly vexing problem, of some importance in special function theory, has been finding the correct $\mathsf{so}(4)$ formulation for the *elliptical* pixellation of a finite 2-dim screen, since such beams have been described and produced with laser arrangements with lenses and masks [17]. And fundamentally, we would like to connect these results with quantum computation.

Appendix: The phase space of finite systems

Figures 8.2 and 8.3 helped us to see the deformations of phase space wrought by aberrations on a rectangle-shaped signal, since the deformed signals themselves can hardly be characterized visually. The Wigner quasi-probability distribution function [33,55] does not contain *more* information than the signal itself, but serves to present the information contained in signals in a format better adapted to our senses; phase space is the music sheet of Hamiltonian systems. The original quantum-mechanical Wigner function [55], still the most used, associates to every wavefunction $\psi(x)$, $x \in \mathsf{R}$, (up to a phase) the real quadratic form [45]

$$W(\psi \,|\, x,\, p) := \int_{\mathsf{R}} \mathrm{d}x'\, \psi(x - \tfrac{1}{2}x')^*\, \exp(-2\pi \mathrm{i}\, x' p)\, \psi(x + \tfrac{1}{2}x'). \qquad (10.1)$$

This form is covariant with translations $e^{-\mathrm{i}ax}\psi(x-b)$ and with linear canonical transformations [27]. We have proposed [1] the definition of a Wigner function that is covariant

under a large class of Lie groups G of dimension D, $W(\mathbf{F}|\mathbf{z})$, $\mathbf{z}\in\mathsf{R}^D$, for functions $\mathbf{F}$ on irreducible representation spaces of G. Here we recall only the case of $\mathsf{SO}(3)$, that is adapted for discrete, finite signals [6].

We ask for $\mathsf{SO}(3)$-covariance between a classical function on $\mathsf{SO}(3)\otimes\mathsf{R}^3$,

$$D_{\rm cl}(\rho,\theta,\phi;x,p,\kappa):=\exp[-{\rm i}(ux{+}vp{+}w\kappa)],\quad \left\{\begin{array}{l} u\,=\rho\sin\theta\sin\phi,\\ v\,=\rho\sin\theta\cos\phi,\\ w=\rho\cos\theta.\end{array}\right. \tag{10.2}$$

and the $N\times N$ matrix representation D^j of $\mathsf{SO}(3)$ generated by the matrices (8.2)–(8.4),

$$D^j_{m,m'}[\rho,\theta,\phi]:=(\exp[-{\rm i}(u\mathbf{X}+v\mathbf{P}+w\mathbf{K})])_{m,m'}, \tag{10.3}$$

where the square brackets on the argument of $D^j_{m,m'}$ indicate that it depends on the *polar* parameters of $\mathsf{SO}(3)$. We attain covariance by building the generating function between the two objects through integration over the $\mathsf{SO}(3)$ group manifold,

$$W^j_{m,m'}(x,p,\kappa):=\frac{1}{|\mathsf{SO(3)}|}\int_{\rm SO(3)}{\rm d}^{\rm Haar}_{\rm SO(3)}[\rho,\theta,\phi]\,D^j_{m,m'}[\rho,\theta,\phi]\,D_{\rm cl}(\rho,\theta,\phi;x,p,\kappa)^* \tag{10.4}$$

with the Haar measure for polar coordinates,

$${\rm d}^{\rm Haar}_{\rm SO(3)}[\rho,\theta,\phi]=\tfrac{1}{2}\sin^2\tfrac{1}{2}\rho\,{\rm d}\rho\,\sin\theta\,{\rm d}\theta\,{\rm d}\phi, \tag{10.5}$$

and the group volume $|\mathsf{SO(3)}|=2\pi^2$.

We can see this *Wigner matrix* $\|W^j_{m,m'}\|$ as a kind of Fourier transform of the Wigner *Big-D* matrices $\|D^j_{m,m'}\|$ [22] that represent the group. The inverse transform involves integrating over '*meta*-phase space' $(x,p,\kappa)\in\mathsf{R}^3$ with $D_{\rm cl}(\rho',\theta',\phi';x,p,\kappa)$. These Wigner Big-$D$ matrices are orthogonal and complete in $[\rho,\theta,\phi]$ and in $\{j;m,m'\}$ with the appropriate measure and weights, and thus the Wigner matrix (10.4) exhibits a host of properties, which include unitarity and hermiticity, 'almost'-positivity, idempotency and marginals, etc. [1]. We find especially interesting the following form in any $\mathsf{SO}(3)$ representation j,

$$\mathbf{W}^j(x,p,\kappa)\;=\;\int_{\rm SO(3)}{\rm d}^{\rm Haar}_{\rm SO(3)}[\rho,\theta,\phi]\;\exp{\rm i}[u(x{-}\mathbf{X}){+}v(p{-}\mathbf{P}){+}w(\kappa{-}\mathbf{K})] \tag{10.6}$$

$$\text{``}\;\approx\;\text{''}\,\delta_{\rm SO(3)}(x-\mathbf{X})\;\delta_{\rm SO(3)}(p-\mathbf{P})\;\delta_{\rm SO(3)}(\kappa-\mathbf{K}), \tag{10.7}$$

i.e., as if the matrices were classical quantities in a 'group-Dirac-δ'. We should also expect that on the sphere $x^2+p^2+\kappa^2\approx j(j{+}1)$ the matrix elements of (10.6) be largest [6].

Now, given a signal N-vector $\mathbf{F}=\{F_m\}^j_{m=-j}$ ($N=2j+1$), or a density matrix $\mathbf{R}=\{R_{m,m'}\}^j_{m,m'=-j}$, their $\mathsf{SO}(3)$ Wigner *function* is the expectation value of $\mathbf{W}^j(x,p,\kappa)$ in the pure or entangled state $\mathbf{F}$ or $\mathbf{R}$, namely

$$W^j_{\rm SO(3)}(\mathbf{F}\,|\,x,p,\kappa\,):=\,\mathbf{F}^\dagger\,\mathbf{W}^j(x,p,\kappa)\,\mathbf{F}=\sum_{m,m'=-j}^{j}F^*_m\,W^j_{m,m'}(x,p,\kappa)\,F_{m'}, \tag{10.8}$$

$$W^j_{\mathrm{SO}(3)}(\mathbf{R}\,|\,x,p,\kappa\,) \;:=\; \text{trace}\,[\mathbf{R}\,\mathbf{W}^j(x,p,\kappa)]. \tag{10.9}$$

The integral (10.4) over the group manifold $[\rho,\theta,\phi]$ must be computed to find the Wigner matrix elements $W^j_{m,m'}(x,p,\kappa)$ on meta-phase space. When we write these in spherical coordinates $[r,\beta,\gamma]$ referred to the x-axis [*cf.* (10.2) with cyclic permutation of axes]

$$p = r\sin\beta\sin\gamma, \quad \kappa = r\sin\beta\cos\gamma, \quad x = r\cos\beta, \tag{10.10}$$

the dependence of the Wigner function on the sphere (β,γ) is separated [6], and we can slice the function at $r^2 \approx j(j+1)$, reducing (10.8) to

$$W^j_{m,m'}[r,\beta,\gamma] = e^{-\mathrm{i}(m-m')\gamma}\sum_{\bar m=-j}^{j} d^j_{m,\bar m}(\beta)\,\overline{W}^{(j)}_{\bar m}(r)\,d^j_{\bar m,m'}(-\beta), \tag{10.11}$$

leaving the elements of the diagonal matrix $\overline{W}^j_{\bar m}(r)$ as functions of only the chosen r. They are reduced to the evaluation of a single sum and integral [6],

$$\begin{aligned}\overline{W}^{(j)}_{\bar m}(r) \;&=\; (-1)^{2j+1}\frac{\pi}{2}\sum_{m=-j}^{j}\int_0^\pi \sin\theta\,\mathrm{d}\theta \\ &\qquad\times |d^j_{\bar m,m}(\theta)|^2\,\frac{\sin(2\pi r\cos\theta)}{(r\cos\theta-m)[(r\cos\theta-m)^2-1]}.\end{aligned} \tag{10.12}$$

These N constants can be evaluated analytically, but we have found it convenient, when producing Figs. 8.2 and 8.3, to compute them numerically and store the values for plotting (10.11) in [64] and here.

The music sheet of a finite signal is thus spherical. This is a bit inconvenient, so we project its (β,γ) coordinates in (10.10) that are referred to the x-axis, onto the plane $0 \le \beta \le \pi$, $-\pi < \gamma \le \pi$, as shown in Figure 10.1. The virtue of this projection is that the the bottom pole of least energy $\kappa \approx -r$, $(\beta,\gamma) = (\frac{1}{2}\pi, 0)$, lies at the center of the rectangle, where the tangency occurs between the sphere and the classical phase space plane. The top pole sits at $(\frac{1}{2}\pi, \pm\pi)$, the x-axis grows from (π,γ) to $(0,\gamma)$, and the p axis grows from $(\frac{1}{2}\pi, -\frac{1}{2}\pi)$ to $(\frac{1}{2}\pi, \frac{1}{2}\pi)$. Under $\mathsf{SO(3)}$ transformations the surface (β,γ) of the sphere rotates rigidly, but $\mathsf{U}(N)$ aberrations deform this manifold. An aberration power monomial of the first pyramid (8.7), $M^{r,\mu;0}(x,p)$, will generate a flow of the surface (β,γ) at the intersection of the sphere with the cylinders $M^{r,\mu;0}(x,p) =$ constant; when this constant is zero, we see that $x = 0 = p$ correspond to planes that separate the flow into quadrants, as shown on the left of Fig. 10.1. Aberrations in the second pyramid (8.8), $M^{r,\mu;1}(x,p,\kappa)$, generate flows that are separated by the $\kappa = 0$ plane into octants, as shown on the right. The flux lines on the sphere and on the plane coincide at the bottom pole for all corresponding aberrations, but at the top pole of highest energy, the $M^{r,\mu;0}$'s and the $M^{r,\mu;1}$'s generate flows in opposite directions.

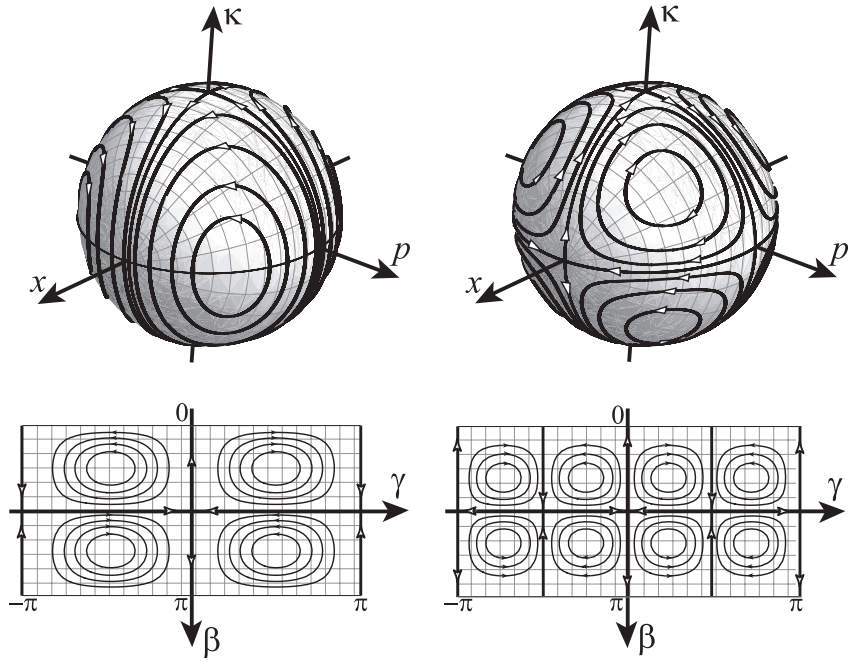

Figure 10.1: Projection of the coordinates (β, γ) of the sphere (*top*), refered to the x-axis in metaphase space $(x, p, \kappa) \in \mathsf{R}^3$, and the lines of flow produced by aberrations, onto the plane (*bottom*). The bottom pole falls on the center of the rectangle, the left and right edges are understood as contiguous, and the top and bottom edges represent a single point on the x-axis. Aberrations $M^{r,\mu;0}(x,p)$ in the first pyramid (8.9), divide the flow into quadrants of nested lines (*left*), while those $M^{r,\mu;1}(x,p,\kappa)$ in the second pyramid divide the flow on the sphere into octants.

I consider important to investigate applications for the group-covariant Wigner operator and quasiprobability distribution function [1]. For the three-parameter Heisenberg-Weyl group we have the partitura of polychromatic wavefields [61], where the Wigner function is drawn with the extra dimension of wavelength; the affine group used for radar detection [21] was the main subject of Ref. [1] because its right- and left-invariant Haar measures are different. For the Euclidean group $\mathsf{ISO}(2)$ the music sheets were written on cylinders [43], and for $\mathsf{SO}(3)$ the results are in this essay. We expect that for $\mathsf{SO}(2,1)$, phase space will be a a two- and one-sheeted hyperboloid for the complementary and principal series, respectively.

We should be aware that there are several Wigner functions on the market, defined for various purposes. For finite systems where the Fourier transform FFT algorithm is used, where positions and momenta are placed on two circles, the natural phase space is the discrete torus [44, 72]; but there, a fractional Fourier transform cannot be implemented globally on this manifold due to the topological obstruction of the hole [69]. The phase

space sphere on the other hand, rotates rigidly around the κ-axis of Figure 10.1; Fresnel and squeezing transforms have the same problem on the torus, but are continuous deformations —aberrations— of the surface of the sphere [70, 71]. For Hamiltonian systems living on a hyperboloid or on a sphere, a Wigner function construction has been proposed by Pogosyan *et al.* [4,5]. And further, a Wigner function for Helmholtz wavefields [68] has led to fundamental advances in radiometry by Alonso *et al.* [2,3,47,53], and Klein-Gordon wavefields will follow suit [46].

Acknowledgements

I thank Professor Mahmoud Abdel-Aty for the invitation to participate in the International Conference on Mathematics and Information Security (Sohag, Egypt, November 13–15, 2009), and acknowledge the support given to the *Óptica Matemática* projects (DGAPA-UNAM IN-105008 and SEP-CONACYT 79899), commending Guillermo Krötzsch and Luis Edgar Vicent (ICF-UNAM) for their help with the algorithms and graphics.

References

[1] S.T. Ali, N.M. Atakishiyev, S.M. Chumakov, and K.B. Wolf, The Wigner function for general Lie groups and the wavelet transform, *Ann. H. Poincaré* **1** (2000), 685–714.

[2] M.A. Alonso, Measurement of Helmholtz wave fields, *J. Opt. Soc. Am. A* **17** (2000), 1256–1264.

[3] M.A. Alonso, Radiometry and wide-angle wave fields. I. Coherent fields in two dimensions, *J. Opt. Soc. Am. A* **18** (2001), 902–909.

[4] M.A. Alonso, G.S. Pogosyan and K.B. Wolf, Wigner functions for curved spaces. I: On hyperboloids, *J. Math. Phys.* **43** (2002), 5857–5871.

[5] M.A. Alonso, G.S. Pogosyan and K.B. Wolf, Wigner functions for curved spaces. II: On spheres, *J. Math. Phys.* **44** (2003), 1472–1489.

[6] N.M. Atakishiyev, S.M. Chumakov, and K.B. Wolf, Wigner distribution function for finite systems, *J. Math. Phys.* **39** (1998), 6247–6261.

[7] N.M. Atakishiyev, A.U. Klimyk and K.B. Wolf, Finite q-oscillator, *J. Phys. A* **37** (2004), 5569–5587.

[8] N.M. Atakishiyev, A.U. Klimyk, and K.B. Wolf, Discrete quantum model of the harmonic oscillator, *J. Phys/ A* **41** (2008), art. 085201, 14p. .

[9] N.M. Atakishiyev, Sh.M. Nagiyev, L.E. Vicent and K.B. Wolf, Covariant discretization of axis-symmetric linear optical systems. *J. Opt. Soc. Am. A* **17** (2000), 2301–2314.

[10] N.M. Atakishiyev, G.S. Pogosyan, L.E. Vicent and K.B. Wolf, Finite two-dimensional oscillator. I: The Cartesian model, *J. Phys. A* **34** (2001), 9381–9398.

[11] N.M. Atakishiyev, G.S. Pogosyan, L.E. Vicent and K.B. Wolf, Finite two-dimensional oscillator. II: The radial model, *J. Phys. A* **34** (2001), 9399–9415.

[12] N.M. Atakishiyev, G.S. Pogosyan and K.B. Wolf, Contraction of the finite one-dimensional oscillator, *Int. J. Mod. Phys. A* **18** (2003), 317–327.

[13] N.M. Atakishiyev, G.S. Pogosyan and K.B. Wolf, Contraction of the finite radial oscillator, *Int. J. Mod. Phys. A* **18** (2003), 329–341.

[14] N.M. Atakishiyev, G.S. Pogosyan, and K.B. Wolf, Finite models of the oscillator, *Phys. Part. Nuclei, Suppl. 3,* **36** (2005), 521–555.

[15] N.M. Atakishiyev and S.K. Suslov, Difference analogs of the harmonic oscillator, *Theoret. and Math. Phys.* **85** (1991), 1055–1062.

[16] N.M. Atakishiyev and K.B. Wolf, Fractional Fourier-Kravchuk transform, *J. Opt. Soc. Am. A* **14** (1997), 1467–1477.

[17] M.A. Bandres and Julio C. Gutiérrez-Vega, Elliptical beams, *Opt. Express* **16** (2008), 21087–21092.

[18] V. Bargmann, Irreducible unitary representations of the Lorentz group, *Ann. Math.* **48** (1947), 568–642.

[19] L. Barker, Ç. Candan, T. Hakioğlu, A. Kutay, and H.M. Ozaktas, The discrete harmonic oscillator, Harper's equation, and the discrete fractional Fourier transform, *J. Phys. A* **33** (2000), 2209–2222.

[20] D. Basu and K.B. Wolf, The unitary irreducible representations of SL(2,R) in all subgroup reductions, *J. Math. Phys.* **32** (1982), 189–205.

[21] J. Bertand and P. Bertrand, A class of Wigner functions with extended covariance properties, *J. Math. Phys.* **33** (1992), 2515–2527.

[22] L.C. Biedenharn and J.D. Louck, *Angular Momentum in Quantum Physics*, Encyclopedia of Mathematics and Its Applications, Vol. 8, Ed. by G.-C. Rota, Addison-Wesley Publ. Co., Reading, Mass., 1981.

[23] S.A. Collins Jr., Lens-system diffraction integral written in terms of matrix optics, *J. Opt. Soc. Am.* **60** (1970), 1168–1177.

[24] A.J. Dragt, Elementary and advanced Lie algebraic methods with applications to accelerator design, electron microscopes, and light optics, *Nucl. Instr. Meth. Phys. Res. A* **258** (1987), 339–354.

[25] A.J. Dragt, E. Forest and K.B. Wolf, Foundations of a Lie algebraic theory of geometrical optics. In: *Lie Methods in Optics*, J. Sánchez Mondragón and K.B. Wolf Eds. Lecture Notes in Physics Vol. 250, Springer Verlag, Heidelberg, 1986.

[26] A. Frank and P. Van Isacker, *Algebraic Methods in Molecular and Nuclear Structure Physics*, John Wiley, New York, 1998.

[27] G. García-Calderón and M. Moshinsky, Wigner distribution functions and the representation of canonical transformations in quantum mechanics, *J. Phys. A* **13** (1980), L185–L190.

[28] I.M. Gel'fand and M.L. Tsetlin, Finite-dimensional representations of the group of unimodular matrices, *Dockl. akad. Nauk SSSR* **71** (1950), 825-828; English translation in *I.M. Gel'fand, Collected Papers*, Vol. II, Springer-Verlag, Berlin, 1987, pp. 653–656.

[29] R. Gilmore, *Lie Groups, Lie Algebras, and Some of Their Applications*, John Wiley, New York, 1974.

[30] I.S. Gradshteyn and I.M. Ryzhik, *Table of Integrals, Series, and Products* Sixth Ed. , Academic Press, 2000.

[31] T. Hakioğlu and K.B. Wolf, The canonical Kravchuk basis for discrete quantum mechanics, *J. Phys. A* **33** (2000), 3313-3324.

[32] J.J. Healy and J.T. Sheridan, Fast linear canonical transforms, *J. Opt. Soc. Am. A* **27** (2010), 21–30.

[33] M. Hillery, R.F. O'Connel, M.O. Scully, and E.P. Wigner, Distribution functions in physics: fundamentals, *Phys. Rep.* **259** (1984), 121–167.

[34] M.L. Mehta,Eigenvalues and eigenvectors of the finite Fourier transform, *J. Math. Phys.* **28** (1987), 781–785.

[35] W. Miller Jr., *Symmetry and Separation of Variables*, , Encyclopedia of Mathematics and Its Applications, Vol. 4, Ed. by G.-C. Rota, Addison-Wesley Publ. Co., Reading, Mass., 1981.

[36] M. Moshinsky and C. Quesne, Oscillator systems. In: *Proceedings of the 15th Solvay Conference in Physics (1970)* , Gordon and Breach, New York, 1974.

[37] M. Moshinsky and C. Quesne, Linear canonical transformations and their unitary representation, *J. Math. Phys.* **12** (1971), 1772–1780.

[38] M. Moshinsky, T.H. Seligman and K.B. Wolf, Canonical transformations and the radial oscillator and Coulomb problems, *J. Math. Phys.* **13** (1972), 901–907.

[39] C.A. Muñoz, J. Rueda-Paz and K.B. Wolf, Discrete repulsive oscillator wavefunctions, *J. Phys. A* **42** (2009), 485210, 12*pp*.

[40] C.A. Muñoz, J. Rueda-Paz and K.B. Wolf, Discrete repulsive oscillator wavefunctions, *J. Phys. A* **41** (2009), art. 485210.

[41] C.A. Muñoz, J. Rueda-Paz and K.B. Wolf, Fractional discrete q-Fourier transforms, *J. Phys. A* **42** (2009), art. 355212 (12 p.).

[42] M.A. Naĭmark, *Linear Representations of the Lorentz Group*, Pergamon Press, Oxford, 1964.

[43] L.M. Nieto, N.M. Atakishiyev, S.M. Chumakov, and K.B. Wolf, Wigner distribution function for Euclidean systems, *J. Phys. A* **31** (1998), 3875–3895.

[44] J.C. O'Neill and W.J. Williams, Shift covariant time-frequency distributions of discrete signals, *IEEE Trans. Signal Process.* **47** (1999), 133–146.

[45] H.M. Ozaktas, Z. Zalevsky, and M. Alper Kutay, *The Fractional Fourier Transform with Applications in Optics and Signal Processing*, Wiley, Chichester, 2001.

[46] J. Petrucelli, Ph.D. Thesis (University of Rochester, USA, 2010).

[47] J.C. Petruccelli and M.A. Alonso, Ray-based propagation of the cross spectral density, *J. Opt. Soc. Am. A* **25** (2008), 1395–1405.

[48] S.-C. Pei and J.-J. Ding, Closed-form discrete fractional and affine transforms, *IEEE Trans. Signal Process.* **48** (2000), 1338–1353.

[49] S.-C. Pei and M.-H. Yeh, Improved discrete fractional transform, *Opt. Lett.* **22** (1997), 1047–1049.

[50] W.P. Schleich, *Quantum Optics in Phase Space*, Wiley-Interscience, Berlin, 2001.

[51] R. Simon and K.B. Wolf, Fractional Fourier transforms in two dimensions, *J. Opt. Soc. Am. A* **17** (2000), 2368–2381.

[52] L.E. Vicent, *Análisis de Señales Discretas Finitas mediante el Modelo de Oscilador Finito de* su(2), Ph.D. dissertation, Universidad Autónoma del Estado de Morelos, 2007.

[53] L.E. Vicent and M.A. Alonso, Generalized radiometry as a tool for the propagation of partially coherent fields, *Opt. Commun.* **207** (2002), 101–112.

[54] L.E. Vicent and K.B. Wolf, Unitary transformation between Cartesian- and polar-pixellated screens, *J. Opt. Soc. Am. A* **25** (2008), 1875–1884.

[55] E.P. Wigner, On the quantum correction for thermodynamic equilibrium, *Phys. Rev.* **40** (1932), 749–759.

[56] K.B. Wolf, Canonical transforms. II. Complex radial transforms, *J. Math. Phys.* **15** (1974), 2101–2111.

[57] K.B. Wolf, The Heisenberg–Weyl ring in quantum mechanics. In *Group Theory and its Applications, III*, Ed. by E.M. Loebl (Academic Press, Nueva York, 1975), pp. 189–247.

[58] K.B. Wolf, *Integral Transforms in Science and Engineering*, Plenum Publ. Corp., New York, 1979.

[59] K.B. Wolf, Symmetry-adapted classification of aberrations, *J. Opt. Soc. Am. A* **5** (1988), 1226–1232.

[60] K.B. Wolf, Refracting surfaces between fibers, *J. Opt. Soc. Am. A* **8** (1991), 1389–1398.

[61] K.B. Wolf, Wigner distribution function for paraxial polychromatic optics, *Opt. Commun.* **132** (1996), 343–352.

[62] K.B. Wolf, Discrete and finite fractional Fourier transforms. In: *Proceedings of the Workshop on Group Theory and Numerical Methods* (Université de Montréal, 26–31 May 2003), *CRM Proceedings and Lecture Series* Vol. **39**, 267–276 (2004).

[63] K.B. Wolf, *Geometric Optics on Phase Space* (Springer-Verlag, Heidelberg, 2004).

[64] K.B. Wolf, Linear transformations and aberrations in continuous and in finite systems, *J. Phys. A* **41** (2008), art. 304026 (19 p.).

[65] K.B. Wolf, Mode analysis and signal restoration with Kravchuk functions, *J. Opt. Soc. Am. A* **26** (2009), 509–516.

[66] K.B. Wolf and F. Aceves de la Cruz, Dependence of s-waves on continuous dimension: The quantum oscillator and free systems, *Fortsch. Physik* **54** (2006), 1083–1108.

[67] K.B. Wolf and T. Alieva, Rotation and gyration of finite two-dimensional modes, *J. Opt. Soc. Am. A* **25** (2008), 365–370.

[68] K.B. Wolf, M.A. Alonso and G.W. Forbes, Wigner functions for Helmholtz wavefields, *J. Opt. Soc. Am. A* **16** (1999), 2476–2487.

[69] K.B. Wolf and G. Krötzsch, Geometry and dynamics in the fractional discrete Fourier transform, *J. Opt. Soc. Am. A* **24** (2007), 651–658.

[70] K.B. Wolf and G. Krötzsch, Geometry and dynamics of the Fresnel transform in finite systems, *J. Opt. Soc. Am. A* **24** (2007), 2568–2577.

[71] K.B. Wolf and G. Krötzsch, Geometry and dynamics of squeezing in finite systems, *J. Opt. Soc. Am. A* **24** (2007), 2871–2878.

[72] W.K. Wooters, A Wigner-function formulation of finite-state quantum mechanics, *Ann. Phys. (N.Y.)* **176** (1987), 1–21.

Kurt Bernardo Wolf is presently Investigador Titular (equivalent to full professor) at the Universidad Nacional Autónoma de México, which he entered in 1971. He was the first director of Centro Internacional de Ciencias AC (1986-1994), organizing 13 national and international schools, workshops and conferences. He is author of: Integral Transforms in Science and Engineering (Plenum, New York, 1979) and Geometric Optics on Phase Space (Springer-Verlag, Heidelberg, 2004), and has been editor of 12 proceedings volumes. His work includes some 150 research articles in refereed journals, 58 chapters and in extenso contributions to proceedings, two books on scientific typography in Spanish and essays for the general public.